

intruded by dacite sills (Figure 19, p.79). Northward from Clover Basin, vertical to overturned beds of the Snowy Range and Grove Creek formations are intruded by numerous dacite sills in the incompetent shaly horizons.

Along the northern boundary (between "B" and "C", Plate I) the Cambrian Maurice Limestone is the lowest recognizable stratigraphic unit exposed, and thick dacite sills intrude the section as high as the Mississippian Madison Formation. Bedding attitudes along the northern boundary ranged from vertical to overturned to the south:

From a point approximately 1 km east of "C" (Plate I) and continuing along the entire eastern border, the pluton is in contact with Madison Limestone. On traverses up Lower Deer Creek (eastern border) and Squaw Gulch (southeastern corner), Madison Limestone was the lowest stratigraphic unit encountered in contact with the main intrusion, but poor exposure and colluvium along much of the eastern margin precluded more detailed mapping. Bedding dips are approximately 20° to 50° east along the eastern border.

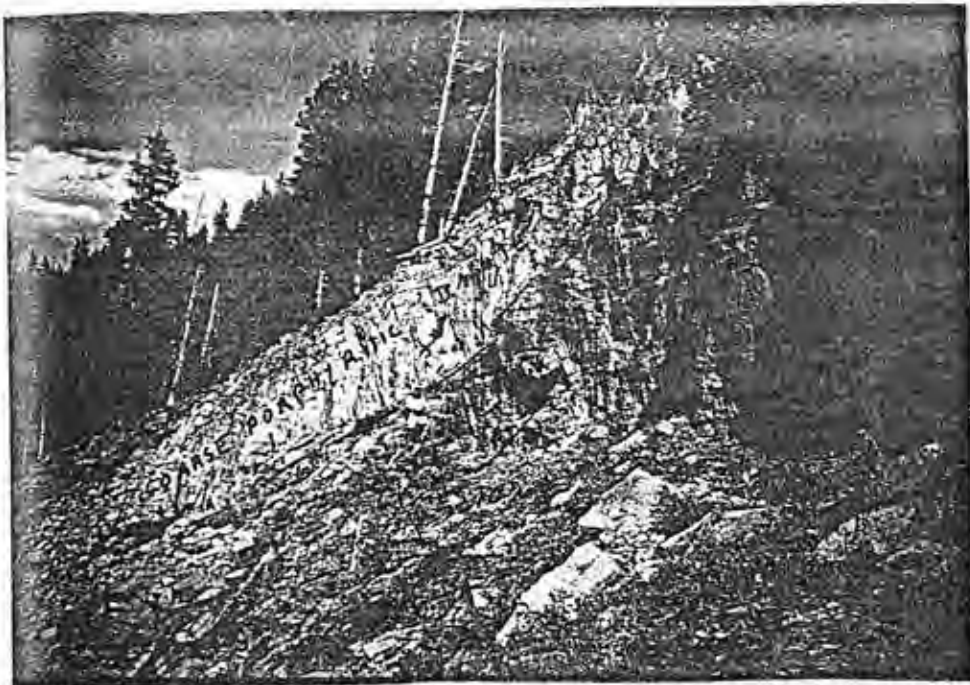
The Jefferson Limestone forms shallowly northward dipping slopes along the southern border of the intrusion. Along the southern border, the slope angle of the north-facing side of the ridge is greater than the dip of the limestone so that the dip projection of the beds is out



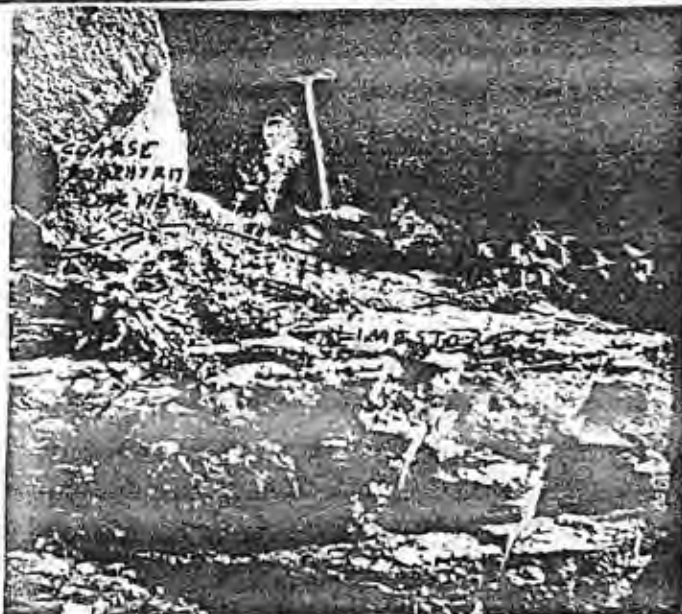
Figure 18. Steeply dipping Jefferson Limestone intruded by marginal sills of coarse porphyritic dacite along western border of Lodgepole Intrusion, 2 km north of Clover Basin. View is toward south. Squaw Peak is labeled.

Figure 19. Coarse porphyritic dacite sill intruded into Snowy Range and Grove Creek formations near the southwest corner of the Lodgepole Intrusion, 0.9 km east of Squaw Peak:

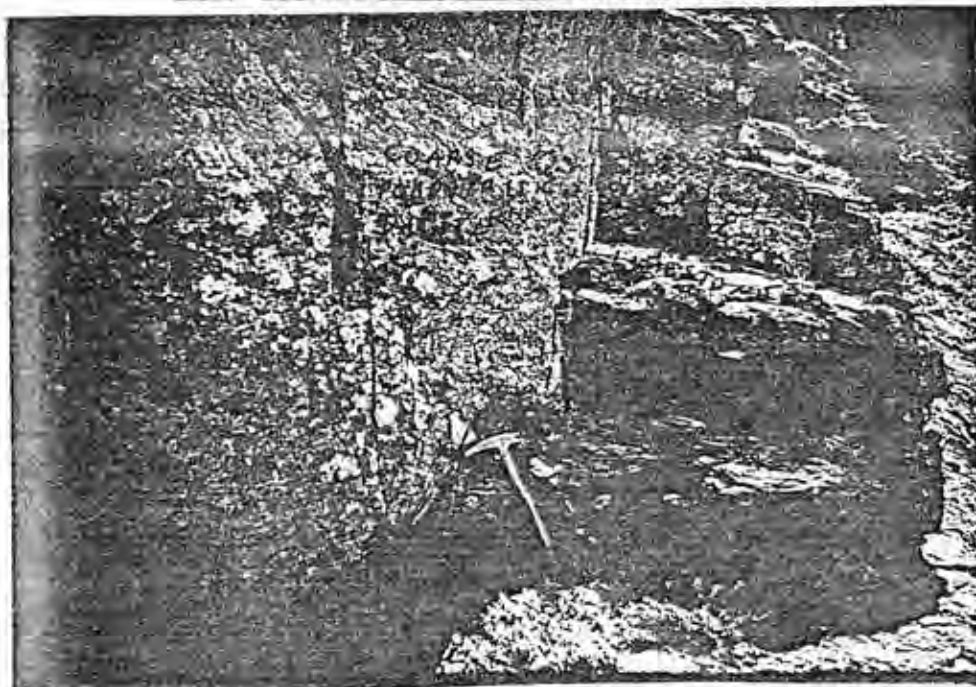
- (a) View is toward southeast. Shallowly northward dipping coarse porphyritic dacite sill (top) intruded into limestone (bottom).
- (b) Porphyry in (a) above is mostly concordant with bedding, as shown in this photo.
- (c) Locally the porphyry shown in (a) above cuts across bedding.



(a)



(b)



(c)

into space toward the area occupied by the intrusion to the north.

Dacite sills project through the ridge which forms the southern border of the main intrusion. These were mapped by Garbarini (1957, p. 126) who reported that sills were abundant in the Cambrian strata on the south-facing slopes of this ridge.

Age Relations

Parsons (1942, p. 1183) states that some of the earliest volcanic breccias on the north side of the Lodgepole Pluton have been upturned by the doming of the north side of the intrusion, along with Cloverly Formation sediments of lower Cretaceous age. These earliest volcanic breccias have been identified as Upper Cretaceous of Montanan age (Judith River Fm. equivalent) based on leaf faunas from a tuff at the base of the volcanic series on the West Branch of Upper Deer Creek, \approx 5 km north of the Lodgepole Intrusion (ibid., p. 1179).

Parsons (1942, p. 1183) also states that later Livingston volcanic breccias unconformably overlie upturned and eroded Cloverly Formation and younger beds on the north side of the Lodgepole Intrusion.

The latest Livingston Formation volcanic breccias and volcanic conglomerates in the area north of the

Lodgepole are conformably overlain by the Hell Creek Member of the Lance Formation (Parsons, 1942, p. 1184), which is the latest Cretaceous formation in the area.

Therefore the age of the Lodgepole Intrusive activity is late Cretaceous, bracketed between the deposition of the Judith River Formation and the Hell Creek Member of the Lance Formation.

Rouse et al. (1937, p. 721) believe that the shape of the Lodgepole Pluton indicates that it was intruded prior to the main Beartooth uplift and compression. They argue that the intrusion most likely would have been elongate E-W had it been intruded after the Beartooth uplift, which resulted in the formation of E-W-trending anticlinal folds in the areas adjacent to the Lodgepole Intrusion.

Garbarini (1957, p. 128) states that dacite sills, "presumably offshoots from the main mass of the Lodgepole Intrusion", found at the head of Blacktail Creek 3.2 km south of the Lodgepole Intrusion, are cut by faults and folds associated with Beartooth uplift and the development of the East Boulder Fault. The timing of the main Beartooth uplift was estimated as Paleocene (middle and late Fort Union) to Eocene (Wasatch) time by Foose et al. (1961, p. 1165).

The above relationships, along with the northward dip of strata along the southern border of the Lodgepole Pluton, place the intrusive event as prior to the development of the East Boulder Fault.

Possible Relationship to Livingston Volcanic Rocks and Initial Depth of Intrusion

From the preceding discussion, it can be seen that intrusion of the main mass of the Lodgepole occurred in late Cretaceous time after deposition of at least the earliest Livingston Volcanic units, because it tilts these breccias (p. 80). Its flanks had been eroded before the end of Cretaceous time (p. 80), because later Livingston Volcanic units unconformably overlie beds upturned by the Lodgepole Intrusion. Therefore, the Lodgepole Intrusion existed as a magma during at least part of the time of extrusion of the Livingston Volcanics and it may have been the source chamber for some of them.

The bulk composition of the central fine-grained diorite facies (p. 68 and Appendix 1-A) also indicates that it could have supplied material for the Livingston Volcanics, because they are dominantly andesitic in composition. The Livingston Volcanics thin rapidly to the north and west from the Deer Creek headwaters region immediately north of the Lodgepole area (Parsons, 1942, p. 1178), from about 610 m to less than 16 m at the Yellowstone River approximately 30 km to the north, indicating a source somewhere near the Lodgepole area.

Using Garbarini's (1957) stratigraphic thicknesses for the McLeod Area (Figure 4, p. 14), from the base of the Bighorn Dolomite (under which the main mass of the Lodge-

pole was intruded) to the top of the Eagle Formation (immediately under the Livingston Volcanic Breccias) a depth of intrusion for the Lodgepole can be calculated as about 2047 m (6715 ft).

This would be a minimum depth because it does not take into account the thickness of volcanic breccias which must have existed at the time of intrusion of the Lodgepole, because the intrusion tilted some of the early breccias (p. 80.)

Using the maximum (2682 m, 8800 ft) and minimum elevations (2073 m, 6800 ft) within the main mass of the intrusion (not including marginal sills), the preserved thickness of the intrusion is at least 610 m (2000 ft).

The massive fine-grained diorite at the western side North of Clover Basin is exposed for a thickness of 445 m (1460 ft) along the steep western side of the diorite outcrop. Xenoliths found at locality "N" (Figure 21, p. 96) occurred near the top of this homogenous diorite massif and were therefore suspended in a considerable thickness of magma at the time of intrusion.

Both of the above thicknesses are minima because an unknown portion of the top of the intrusion has been eroded and the "floor" is not seen.

Although the "floor" of the pluton has been drawn as the Cambrian Flathead Sandstone for purposes of

illustration (Figure 20), the abundance of dacite sills in the Precambrian greenschists and amphibolites along the East Boulder Valley (Figure 12, p.61 and Vail, 1955, Geologic Map) shows that these lithologies were also susceptible to intrusion by the dacite magmas. Therefore, the Lodgepole may not be truly "laccolithic", as it may not have a well-defined floor.

Sequence of Intrusion

A sequence of intrusion based on this author's interpretation of the observed geologic relations (pp. 70-84 is illustrated in Figure 20, p. 88 . (Refer to this figure for the following discussion. Numbers in parenthesis refer to numbered frames in Figure 20).

(1) A sedimentary sequence of Cambrian shales and thin bedded limestones (middle) and massive Ordovician to Mississippian carbonates (top, block pattern) overlies Precambrian greenschists and amphibolites (PGs), showing foliation (S_1). Sediments younger than Mississippian Madison Formation are not schematically represented here.

Site of intrusion may have been localized by existing zones of weakness in the basement (shown at bottom-center) associated with the Nye Bowler Zone, and/or by pre-existing doming (not shown) along the roughly WNW trending Nye Bowler Zone.

- (2) First stages of intrusion of coarse porphyritic dacite magma (small circle pattern). Sills injected dominantly into incompetent shaly horizons in Cambrian interbedded shales and limestones, but sills are also intruded along bedding in the overlying carbonates as high as the Mississippian Madison Formation. Locally limestone inliers (center) are preserved as magma stops its way upward.
- (3) Continued intrusion of coarse porphyritic dacite magma may have been responsible for some initial dip of the marginal sills away from the main pluton. (This dip is schematically shown here on the north edge of the sketch, but is most noticeable in the Lodgepole Intrusion along its eastern boundary.) Lack of fine-grained diorite (discussed in (4)) in the eastern area required another mechanism for tilting the sediments, so some initial dip is proposed here caused by continued intrusion of the dacite.
- (4) Intrusion of fine-grained diorite (stippled pattern), best exposed north of Clover Basin on the west side of the intrusion, causes steepening

of marginal sills along the northern border shown here. Because bedding and marginal sills along the southern border were not steepened, faulting ($f/$) probably broke the strata and allowed more intense deformation to the north side. Material may have been extruded to form some of the Livingston Volcanic rocks during this stage, as discussed previously, but this possibility is not illustrated in this view.

The coarse porphyritic dacite probably was solidified when the diorite was intruded. Evidence for this takes the form of lack of visible evidence of magma mixing or gradational contacts between the dacite and diorite within the intrusion, and the occurrence of fine-grained diorite dikes with nearly vertical contacts in the dacite to the east and northeast of Clover Basin, indicating brittle behavior of the dacite.

Triangles (\blacktriangle) in fine grained diorite schematically represent the abundant xenoliths picked up by the magma on its ascent (discussed on p. 89).

- (5) Uplift along north side of East Boulder Fault about 2 km to the south of the southern end of sketch (not shown here), tilts northern block containing the Lodgepole Intrusion 20° to 30° northward, overturning the already steepened

sediments and marginal sills on the north side of the pluton and causing sediments and sills on the southern border to dip northward at a shallow angle into the intrusion.

(6) Schematic view of present day eroded topography, showing (from south to north):

- ___ Pass Peak, with north dipping Ordovician and Devonian carbonates preserved along ridge crest, and sills of coarse porphyritic dacite penetrating through to south side of ridge.
- ___ Clover Basin area, with remnants of north-dipping carbonates and shales preserved.
- ___ Area N, an abundant xenolith locality (Figure 21, p. 96) in massive peak of fine-grained diorite.
- ___ Steeply north dipping to overturned sediments and marginal porphyritic dacite sills.

Summary of Results (Structure)

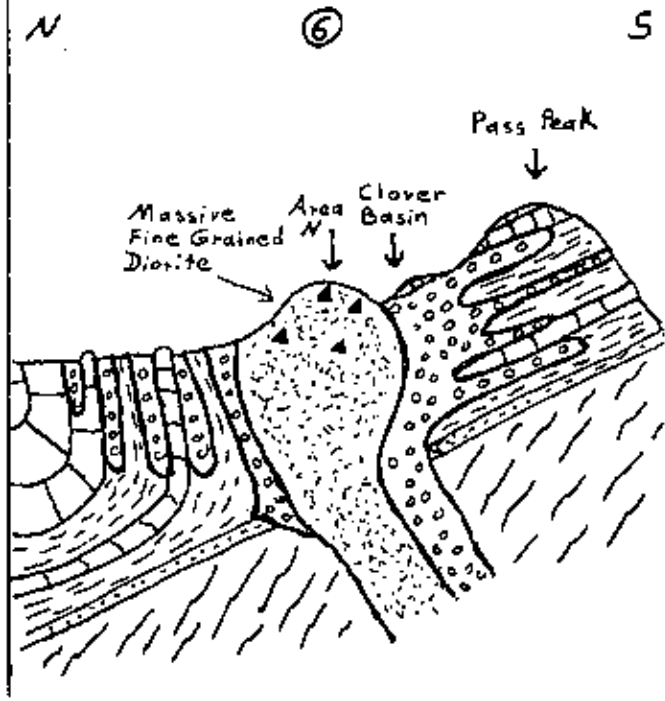
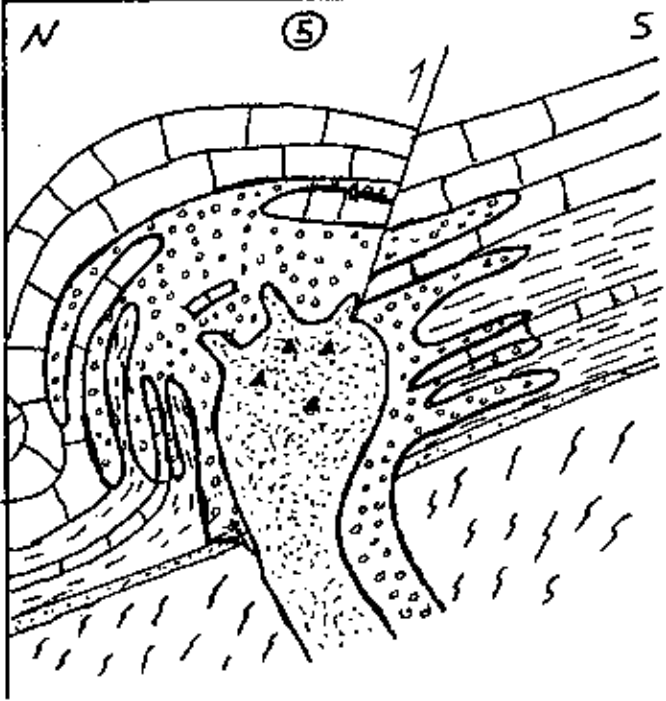
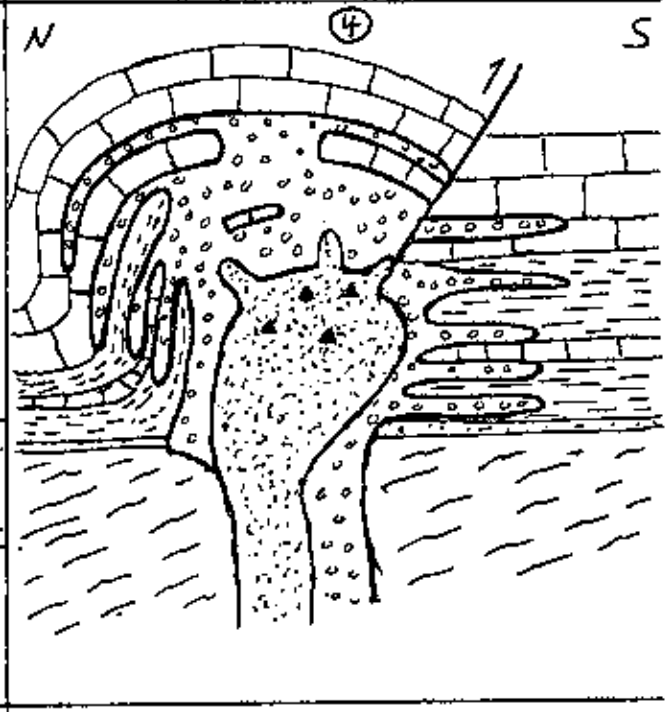
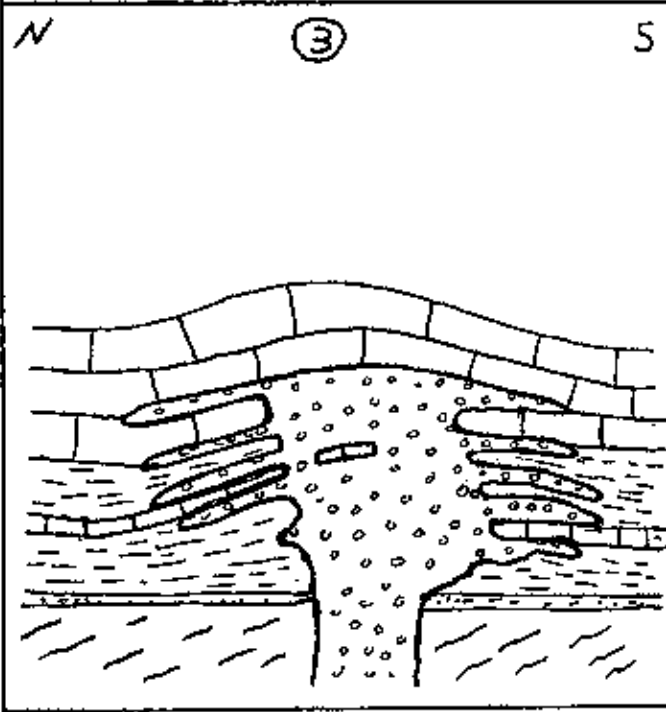
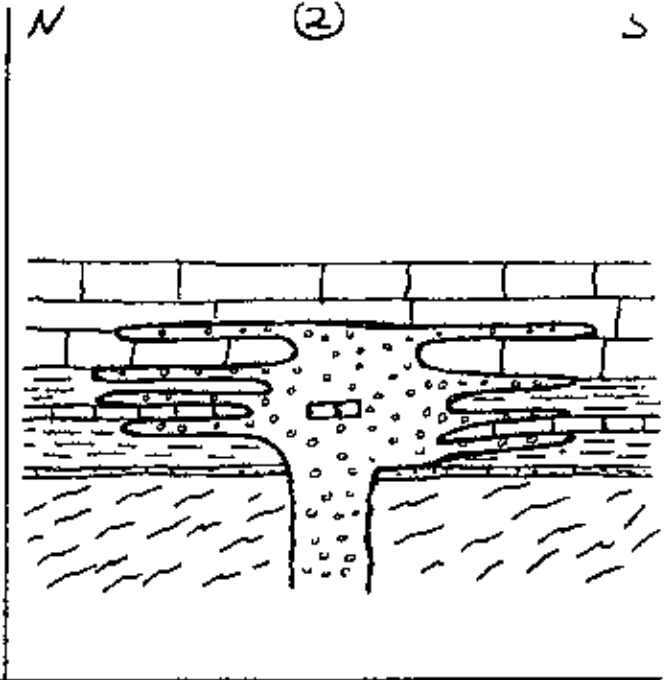
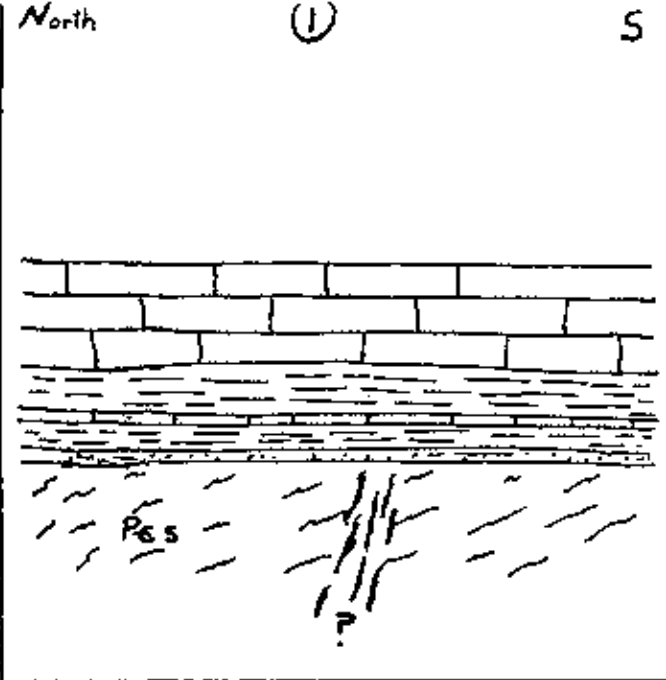
A detailed geologic map of the Lodgepole Intrusion is included as Plate I. The fine-grained diorite is interpreted as a later intrusive phase than the coarse porphyritic dacite because it bowed up and overturned coarse porphyritic dacite sills and sedimentary strata. The abundant occurrences of fine-grained diorite near the Clover Basin area may represent intrusive centers for this phase.

Figure 20.

Schematic cross-sectional representation of sequence of events in the formation of the Lodgepole Intrusive area.

View is along the B - B' cross-section line (Plate II) through the Clover Basin area. Width of each frame (1) through (6) is about 3 km south to north, horizontal and vertical scale approximately equal.

(Refer to text p. 84 for discussion).



Xenoliths in the Lodgepole Intrusion

Xenoliths collected from the Lodgepole Intrusion are listed in Table 5, p.95 . Lithologic names were assigned according to the classification scheme presented in Chapter III, pp. 165-171.

A total of 418 xenoliths were collected. Traverses were set up to attempt to cover all areas of the intrusion, and to sample the xenoliths found in roughly the abundances in which they occurred, although many thousands of xenoliths were observed in the field, no quantitative sampling was attempted.

Geographic Distribution

The location of particularly xenolith-rich areas within the Lodgepole Intrusion are depicted in Figure 21, p. 96.

Area "N" marked the greatest concentration and largest sizes (up to 31 cm in diameter) of cumulate textured plagioclase-containing xenoliths in outcrops of fine-grained diorite (see Figure 25, p.100). Many of the other xenolith lithologies shown in Figure 22, p.97 were also abundant here. Although xenoliths of most lithologies were moderately abundant in the coarse porphyritic dacite near area "N" immediately south of the felsite sill, they were both smaller and less common than within the fine-

grained diorite. Large concentrations of cumulate textured xenoliths (most with matrix still attached) were found in a talus slope of fine-grained diorite marked as area "NE" (see Figure 21, p. 96).

Most of the xenoliths selected for further study because of their size and diversity were found in the "N" and "NE" areas. These samples begin with the letters "N" and "NE" (Table 8, p.119 and Appendix 5). Minor concentrations of cumulate textured xenoliths were also collected from the dike-like areas of fine-grained diorite at "11", "E", and "DC".

The number of xenoliths per unit area seemed to be concentrated by a factor of 10 to 20 in the "N" and "NE" areas relative to other exposures of the fine-grained diorite, and by a factor of at least 20 relative to the large expanses of coarse porphyritic dacite elsewhere in the intrusion. Area 13 marks a minor concentration of xenoliths occurring in coarse porphyritic dacite, but even this large well-exposed area did not contain xenoliths in either the concentration or upper size range of areas "N" and "NE".

All eleven of the garnet (almandine) xenoliths (or xenocrysts) were found scattered in the coarse porphyritic dacite within approximately 0.5 km of the area marked "S". Small (1-3 cm) granular textured dark green amphibolitic

xenoliths, with or without feldspar, were ubiquitous throughout all phases of the pluton.

Xenolith Abundances Relative to Intrusive Phases

The relative abundances of different xenolith lithologies are listed in Table 5, (p.95) and depicted spatially in Figure 22, based on the 418 samples returned from the Lodgepole Intrusion. The distribution of xenoliths relative to the different intrusive phases is shown in Figure 23, p.98 .

About 60% of the xenoliths collected were found in the fine-grained diorite, even though this phase was less abundant in total area (Figure 21, p.96). Considered as a group, 84% of the xenoliths containing cumulate textured plagioclase (Figure 24, p.99) were found in the fine-grained diorite (this group includes the lithologies noted at top left of Figure 22, p. 97). No xenoliths were found in the felsite phase.

While xenoliths containing cumulate textured plagioclase, taken as a group (Figure 24, p.99), showed a greater percentage of samples in the fine-grained diorite phase, certain other groups listed in Table 5, p.95 were more abundant (\geq 60% of the total # of specimens in the class) in the coarse porphyritic dacite:

% of lithology in coarse
porphyritic dacite

chromitite	100% (only 1 sample)
bronzite cumulate (?)	100% (only 4 samples)
diabase	86%
amphibole-plagioclase schist	84%
granular amphibolite	60%
garnet (almandine)	100%.

Note that none of the lithologies with cumulate textured plagioclase (Table 5, p.95 and Figure 24, p.99) were more abundant in the coarse porphyritic dacite (with the exception of mafic norite, which had only one specimen in the class) than in the fine-grained diorite.

Size of Xenoliths

Xenoliths observed ranged in size from 1 cm to 43 cm (a diabase in fine-grained diorite matrix). The largest cumulate textured xenoliths collected were a gabbro (#NE-81-245 = 31 x 25 x 15 cm) and a mafic gabbro (#NE-81-244 = 31 x 31 x 18 cm) both from the "NE" area (Figure 21, p.96 for location of areas), and a gabbroic anorthosite (#N-7(1)-18 = 31 x 16 x 8 cm) from the "N" area. These three xenoliths are illustrated in Figure 25, p. 100.

Using the dimensions for the two cumulate textured samples given above, and the calculated densities listed in Appendix 7 (for interior samples = "IN") the mass of each xenolith is approximately 33.7 kg (=2.90 g/cm³ x

31 cm x 25 cm x 15 cm) for #NE-81-245 and 52.8 kg
($=3.05 \text{ g/cm}^3 \times 31 \text{ cm} \times 31 \text{ cm} \times 18 \text{ cm}$) for #NE-81-244.

This author believes that the large sizes and high relative abundances of xenoliths in the N and NE areas indicates that these areas probably overlie a center of intrusion for the fine-grained diorite.

The mean size of gabbroic anorthosites (an abundant cumulate plagioclase-bearing lithology) was 7.2 cm for samples in the fine-grained diorite, and 2.3 cm for samples in the coarse porphyritic dacite.

The mean size of granular amphibolite (an abundant mafic rich phase without cumulus plagioclase) was 4.0 cm in the fine-grained diorite and 4.3 cm in the coarse porphyritic dacite.

Reaction Rims

Certain lithologies of xenoliths commonly displayed reaction rims that were visible in hand specimens at the contact of the host intrusive and the xenolith (see Chapter III for reaction rim compositions). The following lithologies, as listed in Table 5, p.95 had visible reaction rims on $\geq 40\%$ (arbitrary cut off value)* of the specimens collected:

* see footnote following page.

mottled ultramafic/mafic rocks	41%
chromitite (only 1 sample)	100%
granular amphibolite	40%
sedimentary (carbonate and shale)	75%

The first three lithologies listed above are all composed dominantly of mafic minerals (as discussed in Chapter III).

Roundness/Angularity

Certain lithologies commonly occurred as rounded xenoliths. The following lithologies (from Table 5, p. 95) were "Round" - (no corners visible): in $\geq 40\%$ (arbitrary cut off value) * of the samples:

anorthosite	48%
troctolite	83%
mottled ultramafic/mafic rocks	72%
bronzite cumulate (?)	50%
diabase	50%
amphibole-plagioclase schist	54%
granular amphibolite	90%

Only one class of xenolith (gabbro = 49% Angular) in Table 5 had $\geq 40\%$ of the samples in the "Angular" (= corners sharp and distinct) class.

* cut-off value chosen simply illustrates that some classes of xenoliths commonly have a certain feature. The "40%" value has no inherent quantitative meaning.

Table 5. Lithologies and Abundances of Xenoliths
from the Lodgepole Intrusion

Explanation Key

Xenolith Shape:

R = rounded - no corners visible

SR = subrounded - corners visible but well rounded

SA = subangular - corners distinct but slightly rounded

A = angular - corners sharp and distinct

Host Matrix:

F = fine grained diorite

C = coarse porphyritic dacite

M = medium porphyritic dacite

(percentages listed for "Host Matrix" reflect
only those xenoliths found with attached matrix)

Lithologic names according to classification, Chapter III.

XENOLITHS - LODGEPOLE INTRUSION

Table 5.

Lithology	Number of samples collected	% of total	\bar{x} mean size (cm)	s standard deviation (cm)	number and(%) with megascopically visible reaction rims	Shape				Host Matrix		
						%R	%SR	%SA	%A	%F	C %	M %
Anorthosite	36	8.61	7.4	4.0	2 (6%)	48	16	12	24	69	31	0
Gabbroic anorthosite	82	19.62	7.2	5.9	11 (13%)	31	16	30	23	89	11	0
Gabbro	56	13.40	7.8	6.3	4 (7%)	20	15	16	49	82	14	4
Mafic gabbro	19	4.55	9.3	9.7	0 (0%)	26	21	21	32	79	21	0
Norite	35	8.37	7.5	3.4	5 (14%)	36	11	25	28	93	7	0
Mafic norite	1	0.24	8.0	—	0 (0%)	0	0	1	0	0	100	0
Gabbronorite	6	1.43	7.2	3.4	0 (0%)	0	33.3	33.3	33.3	100	0	0
Troctolite	14	3.35	12.0	4.4	0 (0%)	83	0	17	0	92	8	0
Mottled-ultramafic/mafic rocks	29	6.93	5.0	2.8	12 (41%)	72	12	12	4	34	59	7
Chromitite	1	0.24	3.0	—	1 (100%)	100	0	0	0	0	100	0
Green saussuritized plagioclase	3	0.72	12.0	2.6	1 (33%)	33.3	66.6	0	0	66.6	33.3	0
Bronzite cumulate(?)	4	0.96	3.5	1.0	0 (0%)	50	25	25	0	0	100	0
				(continued)								

XENOLITHS - LODGEPOLE INTRUSION (Cont.d)

Table 5.

Lithology	Number of samples collected	% of total	\bar{x} mean size (cm)	s standard deviation (cm)	number and(%) with megascopically visible reaction rims	Shape				Host Matrix		
						%R	%SR	%SA	%A	%F	%C	%M
Dark green amph. & pink feldspar	4	0.96	3.5	0.6	0 (0%)	25	75	0	0	50	50	0
Diabase	44	10.53	4.9	6.4	0 (0%)	50	27	16	7	14	86	0
Amphibole-plag. schist	13	3.11	4.6	2.8	0 (0%)	54	8	38	0	8	84	8
Granular amphibolite	20	4.78	4.2	2.1	8 (40%)	100	0	0	0	30	60	10
"Hornfels"	5	1.20	4.8	2.0	0 (0%)	20	0	60	20	50	50	0
Garnet	11	2.63	1.1	0.6	0 (0%)	73	27	0	0	0	100	0
Gneiss	18	4.30	7.8	3.2	0 (0%)	31	13	25	31	47	47	6
Granite	11	2.63	7.8	3.1	1 (9%)	18	18	28	36	55	36	9
Sedimentary	4	0.96	5.8	1.9	3 (75%)	75	0	25	0	75	25	0
Intrusive-in-intrusive	2	0.48	9.5	5.0	0 (0%)	50	0	0	50	50	50	0

Total # 418

Figure 21. Outline Geologic Map of the Lodgepole Intrusion

Particularly xenolith rich localities are marked by crosses (+). Size of cross denotes relative abundance of xenoliths for locality. "S" and "13" refer to other areas discussed in text. (see p; 89 , Geographic Distribution of Xenoliths).

Legend:

coarse porphyritic
 dacite = unpatterned(outlying
 coarse porphyritic
 dacite sills marked
 "C")

fine-grained diorite=stippled pattern

felsite sill = "felsite"

latite sill = ✓ pattern

limestone inliers =block pattern

The Clover Basin area is marked by
 a *.

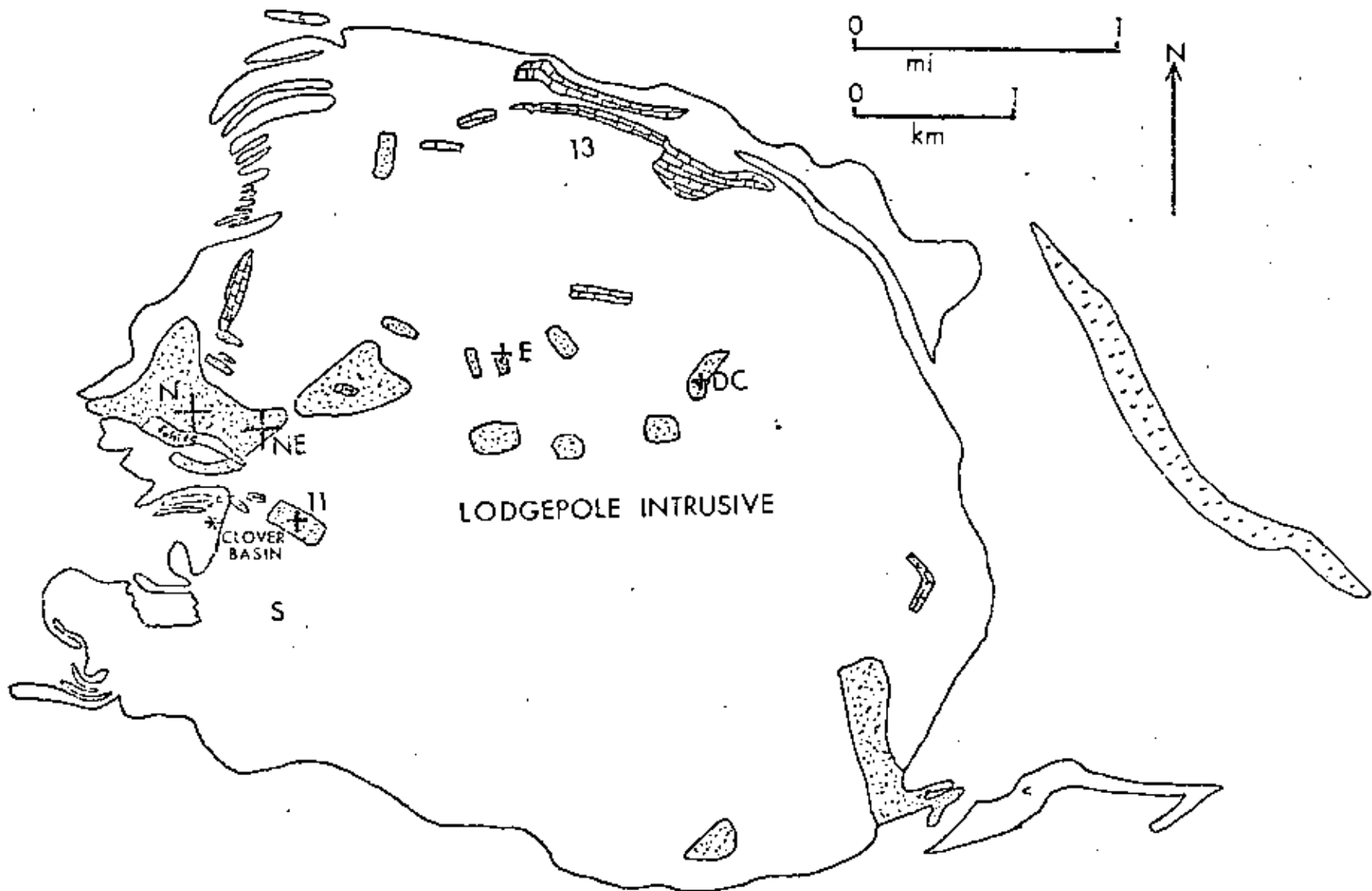


Figure 22. Distribution of Xenoliths by
Lithology for the Lodgepole Intrusion

Lithologic names according to
classification, Chapter III.

Major groupings shown across top
of diagram include from left to right:

- samples containing cumulus
plagioclase.
- ultramafic lithologies exhibiting
cumulate textures (chromitite) or
textures interpreted as relict
cumulate textures (see Chapter III,
P.164).
- diabase.
- granular hornblende and tremolite-
actinolite mafic amphibolites with-
out cumulus plagioclase.

Number of samples

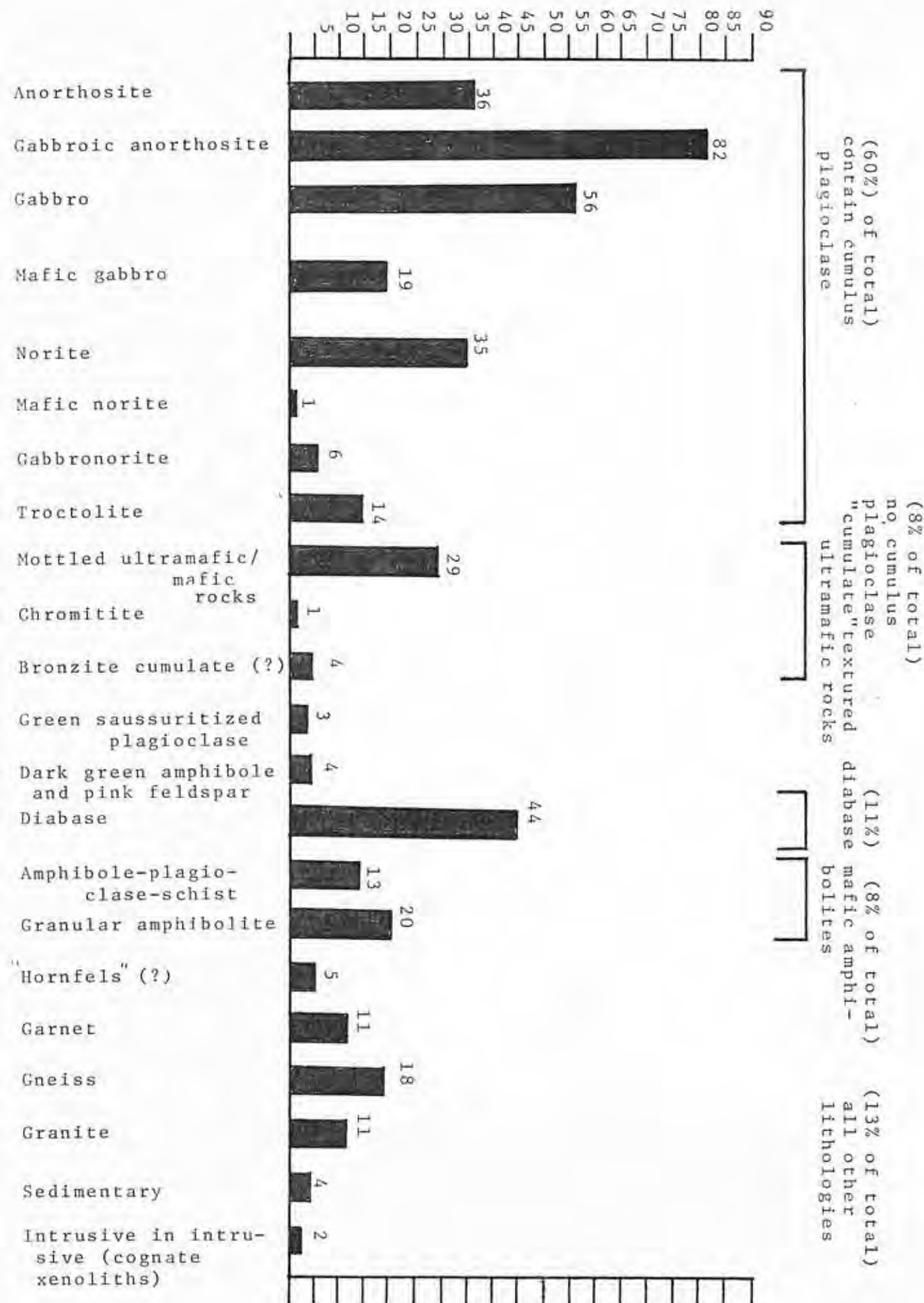


Figure 23.

Lodgepole Intrusion

Percentage of Total Number of Xenolith
Samples Occurring in Each Intrusive Phase

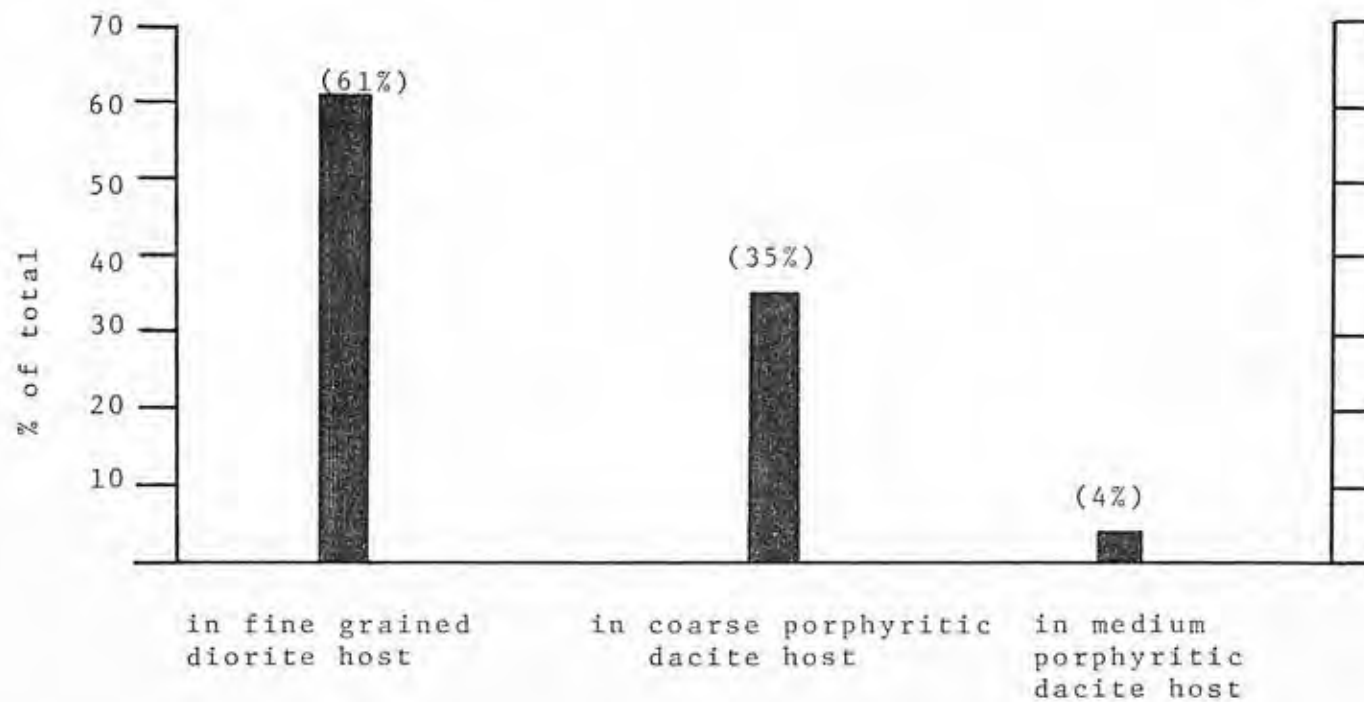


Figure 24.

Lodgepole Intrusion

Percentage of (Xenoliths Containing Cumulate Textured
Plagioclase Considered as a Group)
in Each Intrusive Phase.

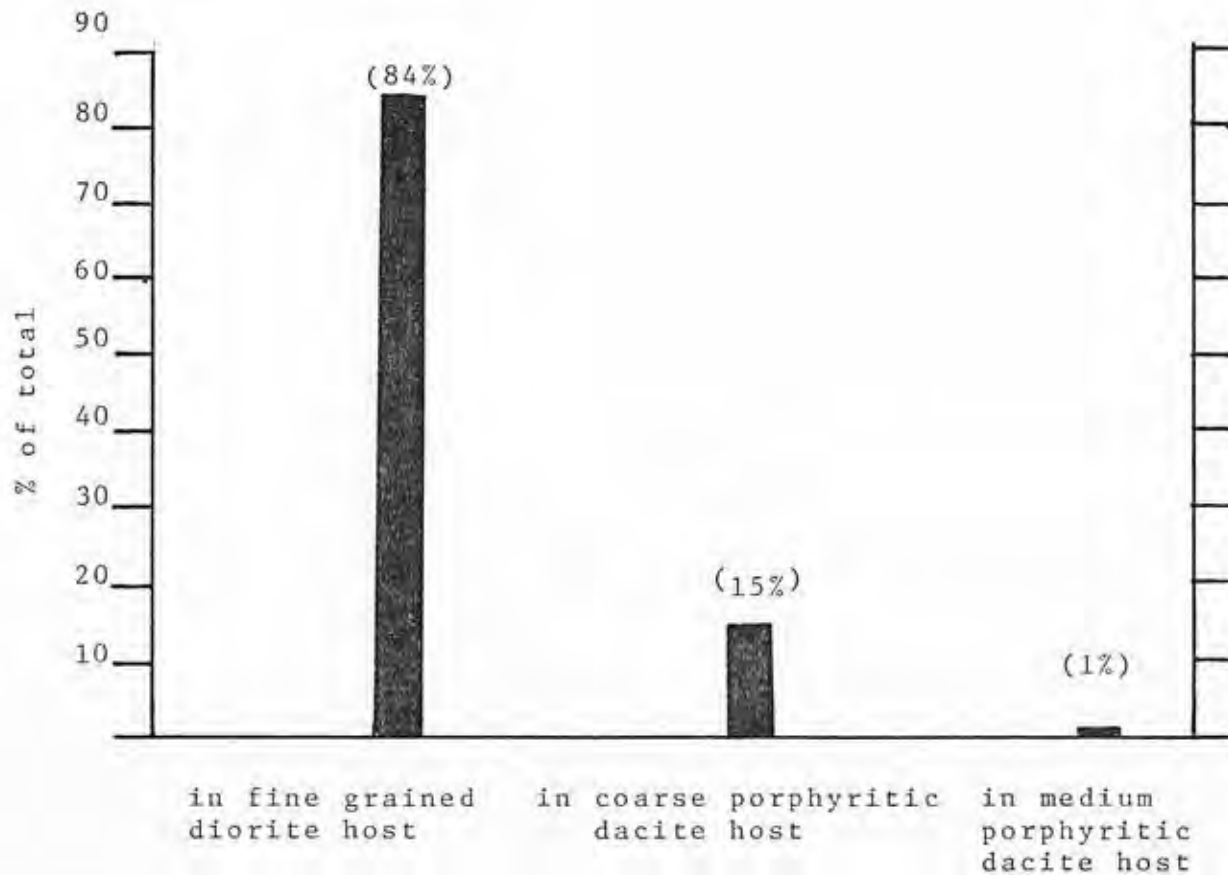


Figure 25.

- (a) Large cumulate textured xenoliths from "NE" talus slope (NE located on Figure 21, p.96). Mafic gabbro NE-81-244 (31 x 31 x 18 cm) is on left above scale, gabbro NE-81-245 (31 x 25 x 15 cm) is on right. Matrix (tan) is fine-grained diorite. (Scale is 15 cm)
- (b) Large gabbroic anorthosite (N-7(1)-18) in outcrop from area N (Figure 21, p. 96). Matrix is fine-grained diorite. (Magnet on left is 13 cm)

Petrographic descriptions are in Appendix 5:

NE-81-244 page 5- 21

NE-81-245 " 5- 17

N-7(1)-18 " 5- 9

See text p.92 for discussion.



(a)



(b)

Summary of Results (Xenoliths)

The occurrence of the largest and most abundant xenoliths in fine-grained diorite localities ("N" and "NE" areas, Figure 21, p. 96.) north of Clover Basin suggests that these areas overlie intrusive centers for the fine-grained diorite. Cumulus plagioclase-bearing xenoliths were most abundant (84% of this group) in the fine-grained diorite phase (Figure 24, p. 99). Mafic mineral-rich xenoliths exhibit reaction rims more commonly than plagioclase-rich lithologies. No restriction of xenolith roundness to a specific lithologic type was noted.

In Chapter IV, the size and density of the largest cumulate textured xenoliths are used to constrain minimum ascent rates for the Lodgepole magma, and the Lodgepole xenoliths are compared with those collected from the Enos Mountain and Susie Peak intrusions.

Section 3

Enos Mountain and Susie Peak Intrusive Areas

ENOS MOUNTAIN AND SUSIE PEAK AREAS

Purpose of Study

A reconnaissance study was conducted in the Enos Mountain and Susie Peak areas for the purpose of evaluating the types and distribution of crystalline basement xenoliths in these igneous rocks.

Geologic Setting

The Enos Mountain and Susie Peak Intrusive-Extrusive Complex covers the area between the headwaters of Elk and Susie Creeks (Plate I, northwest quarter). Geologic relations in the area are complex, with evidence for multiple periods of intrusion, extrusion, and faulting. The reader is referred to Booker (1957) for a detailed geologic map of the sedimentary structures and faults in the area.

Both the Enos Mountain and Susie Peak "intrusions" are actually complex areas of shallow intrusive sills, plugs, dikes, pipes, extrusive breccias, and mud- and water-sorted volcanic agglomerates, separated by the valley of Enos Creek which has cut through some of the bedded agglomerates and into deformed sediments.

Garbarini (1957, p. 131) recognized three general phases of igneous activity in the area:

- (1) Intrusion of sills into flat lying or gently dipping sediments.
- (2) Vent phase volcanism where breccias were ejected and modified by water action (hot and cold mud flows).
- (3) The main plug of non-brecciated porphyry was emplaced southeast of the crest of Enos Mountain and sedimentary strata on the northwest side were tilted and overturned. Faulting also involved the early bedded breccias at Susie Peak and Enos Creek.

Breccias and agglomerates along the north side of Enos Creek (northward dips) and east of the crest of Enos Mountain (eastward dips), thin and dip directly away from an area of massive intrusive rocks southeast of the crest of Enos Mountain. Booker (1957, p. 29) noted this axi-symmetric distribution and suggested it represented a major vent.

Age Relations

Booker (1957, p. 21) proposed to include the volcanic breccias in the Enos area in the Livingston Formation, because his work showed that they overlie the Cretaceous Eagle Formation and therefore correlate with the Upper Member of the Livingston Formation.

Parsons (1942, p. 1178) states that the lowest extrusive breccias in the Enos Mountain area are Upper Cretaceous (Judith River Formation equivalent) based on leaf faunas found in a tuff bed.

This author observed that one of the intrusions in the Susie Peak area (NE 1/4 section 11 on Plate I) cuts the Cretaceous Eagle Formation, and at this locality minor occurrences of coal occur as brittle black anthracolite, (apparently heated by the intrusion) as opposed to the soft brown lignite occurring elsewhere in this formation.

The above observations suggest a late Cretaceous or younger age for the intrusion in the Enos-Susie Peak area. Parsons (1942, p. 1184) states that no evidence of volcanic activity is present in the latest Cretaceous Lance Formation (which overlies the Livingston Volcanic rocks). Therefore it is likely that the Enos-Susie Peak igneous rocks, which are in part extrusive, are of pre-Lance Formation age.

Intrusive-Extrusive Phases

Previous workers in the area have variously classified the igneous breccias, massive porphyries, and agglomerates as andesitic (Booker, 1957, p. 32; Garbarini, 1957, p. 129a) and dacitic (Rouse et al., 1937, p. 724; Parsons, 1942, p. 1178) after describing the same lithologies. Booker (1957) grouped the igneous "auto-breccias" (consisting

of porphyry fragments in a crystal tuff matrix) together with the non-brecciated intrusive porphyries on his map.

The conflict in previous nomenclature of these rocks, and the lack of chemical analysis or extensive petrography, led this author to map the rocks simply as massive intrusive porphyry ("C" on map, Plate I), and extrusive rocks (Klvag on map, Plate I) for the purpose of this study.

The rocks included as intrusive "C" are massive porphyritic sills and plugs similar in hand specimen appearance to the coarse porphyritic dacite described for the Lodgepole Intrusion (p.68).

The rocks included as extrusive (Klvag) cover a wide variety of lithologies including igneous breccias (angular clasts of coarse porphyry in a crystal tuff matrix); crudely bedded water-and-mud-flow-laid agglomerates (both clast-supported and matrix-supported) consisting of porphyry, fine-grained volcanic, and sedimentary clasts; and welded tuffs.

A pipe of fine-grained equigranular andesite was noted in the study area immediately north of the crest of Enos Mountain and is labeled "pipe" on Plate I. This pipe cuts massive porphyritic dacite.

Depths of Intrusion

The layers of dacite ("C") in the Susie Peak area intrude the Cretaceous Eagle Formation, and thin coarse porphyry sills of similar composition were observed in some of the bedded agglomerates attributed to the Enos Vent. The fact that the above intrusions are emplaced in Livingston Volcanic units suggest a shallow subvolcanic depth.

Xenoliths

The "Enos Mountain Intrusive Area" is considered here as the intrusions and vent breccias mapped in Plate I, located south of Enos Creek and North of Elk Creek. The "Susie Peak Intrusive Area" refers to the area of intrusion, agglomerates and tuffs mapped in Plate I lying north of Enos Creek and south of Susie Creek.

The goal of this portion of the study was to concentrate on the collection of xenoliths representing underlying crystalline and metamorphic basement lithologies. The distribution of sedimentary xenoliths and "auto-breccia" clasts (of volcanic clasts within volcanic flows) is mentioned here, but they are not included in Tables 6, and 7, pp. 112 and 113 .

Xenoliths of the Paleozoic and Mesozoic sedimentary rocks are abundant in the porphyritic igneous vent breccias

southeast of the crest of Enos Mountain, especially massive dark grey limestone (Mississippian Madison?) and mottled dolomite (Ordovician Bighorn). In the bedded agglomerates north of Enos Creek, clasts of limestones, dolomites, red shales, and sandstones formed significant percentages of the rocks (up to 20%). Limestone or clastic sedimentary xenoliths were not found in the unbrecciated massive porphyritic intrusive sills on Enos Mountain.

"Autoliths" of the dacitic and andesitic volcanic flows occurred in the bedded volcanic breccias and tuffs north of Enos Creek. Angular clasts of dark red andesite in green andesite, and vice-versa were common. Fragments of the same lithologic type as the coarse porphyritic intrusive sills and massive igneous vent breccia clasts were commonly found in a finer grained tuff matrix, but because thin sills of this same coarse porphyritic lithology cut these tuffs, there was obviously more than one period of intrusion of the coarse porphyry lithology.

Enos Mountain Area - Geographic Distribution and Abundance Relative to Intrusive Phases

The small (≈ 150 m diameter) fine-grained andesite "pipe" north of the crest of Enos Mountain (marked "pipe" on Plate I) marked the most concentrated locality for basement-type xenoliths found in the Enos Mountain Intrusive

area. (15 assorted plagioclase cumulate lithologies and amphibolites). These were all in a fine-grained andesite ("A" in Table 6) matrix (Figure 27, p. 115).

The remaining 25 samples of cumulate textured xenoliths were found widely distributed throughout the massive porphyritic intrusive sills north of the crest of Enos Mountain, and in the igneous porphyry breccias south of the crest of Enos Mountain. These were all found as xenoliths within clasts of the coarse porphyry lithology (rather than loose in the matrix as clasts themselves) and are listed under matrix "C" in Table 6, p. 112.

Size of Xenoliths

The two largest xenoliths included in Table 6 were a 9 cm gabbro and an 8 cm gabbroic anorthosite. Booker (1957, p. 20) reported "anorthositic gabbro boulders" (no exact size) in the Enos Mountain breccias, but no cumulate textured xenoliths larger than mentioned above were found by our party. None of the groups had mean sizes greater than 4.7 cm in diameter (gabbroic anorthosite).

Roundness/Angularity

All groups (except the diabase) listed in Table 6, p. 112 had $\geq 40\%$ of the samples in the "rounded" (shape defined p. 95) class.

Reaction Rims

The mottled ultramafic/mafic rocks and the granular amphibolites listed in Table 6, p. 112, had reaction rims visible in hand specimen on $\geq 40\%$ of the specimens in the class.

Susie Peak Area- Geographic Distribution and Distribution Relative to Intrusive Phases

A concentrated collection (16 samples) of cumulate textured xenoliths was found at locality SP-7 in a fine-grained dark grey andesitic crystal tuff matrix, and at locality SP-10 (6 samples) in dark grey fine-grained andesitic matrix. (Both localities are marked on Plate I. SP-7 is in SW 1/4 Section 1, and SP-10 is in NW 1/4 Section 12, Susie Peak area.

The remainder of the samples (in Table 7, p. 113) were found widely scattered in the massive porphyritic intrusive ("C") phase and in the tuffs and agglomerates.

Figure 28 (p. 116) illustrates a large 2 meter clast of fine-grained andesite in a tuff matrix, showing xenoliths of a gabbro and diabase within the large clast.

Size of Xenoliths

The largest xenoliths included in Table 7, (p. 113) were two gabbroic anorthosites (8 and 6 cm). Gabbro and anorthosite had the largest mean sizes (4.0 cm each).

Reaction Rims

Only the mottled ultramafic/mafic xenoliths had visible reaction rims on $\geq 40\%$ of the class (Table 7, p. 113).

Roundness/Angularity

All lithologies except anorthosite and gabbroic anorthosite had $\geq 40\%$ of their class in the "round" (shape defined, p. 95) category, (Table 7, p.113).

Summary of Results (Enos Mountain/Susie Peak Areas)

Cumulate textured xenoliths occur most commonly in localized areas within the Enos Mountain-Susie Peak Intrusive-Extrusive Complex. Plagioclase cumulate xenoliths up to 9 cm across are most common in an andesitic "pipe" or volcanic plug immediately north of the crest of Enos Mountain, and in a fine-grained dark grey andesitic crystal tuff locality (SP-10) in the Susie Peak area. Mafic mineral-rich xenoliths exhibit reaction rims with the host intrusive phase more commonly than plagioclase-rich xenoliths. No restriction of xenolith roundness to a specific lithologic type was noted.

In Chapter IV, the Enos Mountain - Susie Peak xenoliths are compared with those collected from the Lodgepole Intrusion.

Table 6. XENOLITHS - ENOS MOUNTAIN INTRUSION AREA

Lithology	Number of samples collected	% of total	\bar{x} mean size (cm)	s standard deviation (cm)	number and(%) with megascopically visible reaction rims	Shape *				Host Matrix**		
						%R	%SR	%SA	%A	%C	%A	
cumulate textured	Anorthosite	1	2.50	2.0	--	0 (0%)	100	0	0	0	0	100
	Gabbroic anorthosite	3	7.50	4.7	2.9	1 (33%)	66.6	0	33.3	0	0	100
	Gabbro	7	17.50	3.3	2.6	0 (0%)	43	14	14	29	0	100
	Mafic gabbro	1	2.50	1.0	--	0 (0%)	100	0	0	0	100	0
	Mottled-ultramafic/mafic rocks	8	20.00	2.6	1.1	7 (87%)	87	0	0	13	87	13
Diabase	8	20.00	1.8	0.7	0 (0%)	0	75	12.5	12.5	75	25	
mafic amphibolites	Amphibole-plag. schist	2	5.00	2.0	1.4	0 (0%)	50	0	50	0	100	0
	Granular amphibolite	10	25.00	2.0	1.2	4 (40%)	80	20	0	0	90	10

Total # 40

* shape (defined p. 95)

** Host Matrix: C = massive porphyry lithology
or in clasts of porphyry lithology
(see page 106)
A = fine-grained andesite "pipe"
(see page 106)

Table 7. XENOLITHS - SUSIE PEAK INTRUSION AREA

Lithology	Number of samples collected	% of total	\bar{x} mean size (cm)	s standard deviation (cm)	number and(%) with megascopically visible reaction rims	Shape *				Host ** Matrix	
						%R	%SR	%SA	%A	%C	%A
Anorthosite	6	16.67	4.0	0.9	2 (33%)	17	0	33	50	0	100
Gabbroic anorthosite	7	19.44	3.3	2.8	1 (14%)	28	44	28	0	0	100
Gabbro	2	5.56	4.0	1.4	0 (0%)	50	50	0	0	0	100
Mafic gabbro	5	13.89	3.4	0.6	0 (0%)	80	0	0	20	0	100
Mottled-ultra-mafic/mafic rocks	5	13.89	1.8	0.8	3 (60%)	80	0	0	20	0	100
Diabase	6	16.66	2.0	0.0	1 (17%)	83	0	0	17	67	33
Granular amphibolite	5	13.89	1.6	0.6	1 (20%)	80	20	0	0	100	0

Total # 36

* Shape (defined p. 95)

** Host Matrix: A= fine grained dark grey andesite crystal tuff
C= massive porphyry lithology or in clasts of porphyry lithology

Lithologies according to classification, Chapter III, p. 165.



Figure 26. Bedded agglomerates along north side of Enos Creek (south-center section 12, Plate I). Agglomerates dip 20° - 30° northwest away from Enos Mountain area, and are composed of a variety of fine-grained volcanic and porphyritic igneous clasts as well as sedimentary clasts.

Figure 27.

- (a) Small andesitic "pipe" on north side of Enos Mountain (View is toward south from Susie Peak Area. "Pipe" is noted on map, Plate I). The main vent area proposed by Booker (1957, p. 21) is just beyond the vertical Madison Limestone on the skyline. Diameter of "pipe" (dashed outline) is about 150 m. Cumulate textured xenoliths were abundant in the "pipe" area.
- (b) Small cumulate textured xenoliths found within area of "pipe" (above) are marked by arrows. Light-colored clast to right is limestone.



(a)



(b)

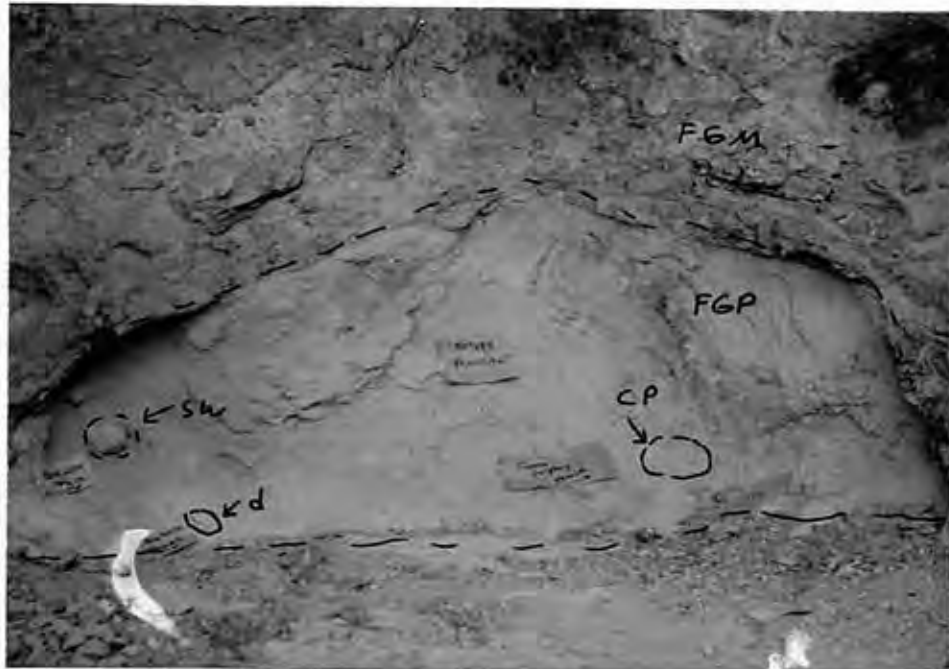


Figure 28. Large fine-grained porphyry (FGP) in fine-grained matrix (FGM) in bedded agglomerates on north side of Enos Creek. Note the xenoliths inside the large (FGP) clast.

sw - cumulate textured gabbroic xenolith
 d - diabase
 cp - coarse porphyry lithology

Large (FGP) clast is 2 meters long.

Chapter III

Xenoliths: Chemistry, Mineralogy, and
Texture

XENOLITHS: CHEMISTRY, MINERALOGY AND TEXTURE

Purpose of Study

Whole rock chemical data are used to illustrate the compositional ranges of the xenoliths and to calculate their normative mineralogies in order to determine their degree of silica saturation. Lithologic names are assigned on the basis of hand sample and thin section petrographic studies, combined with electron microprobe determinations of mineral compositions, as discussed in this chapter. Cumulate textured xenoliths characterized by the above methods are compared with literature data on Stillwater Complex lithologies (Chapter IV).

The xenoliths chosen for detailed study were collected from the Lodgepole Intrusion. They are listed in Table 8 (p. 119). The samples in Table 8 are grouped according to their degree of silica saturation (p.134), and the silica saturated cumulus plagioclase xenoliths are listed in Table 8 in order of decreasing measured An content (App. 4-C). The same sample order is used in Appendices 1 (whole rock chemistry), 2 (trace elements), 3 (normative mineralogy), and 7 (density). Samples chosen appear to represent igneous and metamorphic rocks.

Table 8 Index of Xenolith Samples
 (Samples listed in same order as in Appendices 1 - 3)

Xenolith Lithology	Sample No.	whole rock chemistry and normative mineralogy	information available for each sample: x = yes - = no					
			thin section	electron micro- probe analysis		petrographic description (page #)	hand specimen photograph	photomicrograph (page #)
				plagio- clase	mafic min.			
CIPW Silica Undersaturated mottled ultramafic rock	13-81-227	x	x	-	-	5-41	x	154
gabbroic anorthosite	N-81-166	x	x	x	-	5-8	x	-
anorthosite	NE-81-500	x	x	x	x	5-5	-	-
gabbroic anorthosite	N-7(1)-18	x	x	-	-	5-9	x	-
CIPW Silica Saturated (with cumulus plagioclase)								
norite	NE-81-502	x	x	x	x	5-25	x	151
norite	N-81-110	x	x	x	-	5-26	x	152(rim)
anorthosite	N-81-160	x	x	x	-	5-4	x	139
anorthosite	13-81-229	x	x	x	x	5-3	x	-
gabbro	NE-81-245IN	x	x	x	x	5-17	x	-
norite	TU1-80	x	x	x	-	5-24	x	-
troctolite	N-81-113	x	x	x	-	5-33	x	142
gabbro-norite	N-81-162	x	x	x	x	5-30	x	152
troctolite	N-7(1)-2	x	x	x	x	5-32	x	-
gabbro	E-4	x	x	x	x	5-16	x	-
troctolite	N-7(1)-16	x	x	x	-	5-35	x	155
mafic gabbro	NE-81-501	x	x	x	x	5-20	x	148
gabbro-norite	NE-81-507	x	x	x	x	5-29	x	-

Index of Xenolith Samples (Continued)

Xenolith Lithology	Sample No.	whole rock chemistry and normative mineralogy	thin section	electron microprobe analysis		petrographic description (page #)	hand specimen photograph	photomicrograph (page #)
				plagioclase	mafic min.			
<u>CIPW Silica Saturated (Contd.)</u> (green saussuritized plagioclase + amphibole)								
norite	E-1-B-8	x	x	x	x	5-43	x	156
gabbroic anorthosite	N-81-246	x	x	x	x	5-27	x	-
mafic gabbro	N-80-TU-5	x	x	x	x	5-14	x	-
anorthosite	NE-81-244IN	x	x	x	x	5-21	x	-
troctolite	NE-81-201	x	-	-	-	5-6	x	-
gabbroic anorthosite	N-81-130	x	x	-	-	5-34	x	-
gabbroic anorthosite	N-80-TU-3	x	x	x	-	5-11	x	-
gabbroic anorthosite	N-81-8720A3	x	x	x	x	5-13	x	-
mafic gabbro	N-81-102	x	x	x	-	5-12	x	-
(green saussuritized plagioclase + amphibole)	N-81-203	x	x	-	-	5-22	x	-
	13-81-237	x	x	x	x	5-44	x	-
<u>CIPW Silica Saturated (no cumulus plagioclase)</u>								
granular amphibolite	N-8400A1	x	x	x	x	5-46	x	149
amphibole-plagioclase schist	NE81-508	x	x	-	x	5-50	x	-
mottled ultramafic rock	N81-161	x	x	-	-	5-39	x	-
granular amphibolite	8300 S.Spine	x	x	-	x	5-48	x	-
mottled mafic rock	TR-1(0)-1	x	x	-	x	5-40	x	-
diabase	WCB-1	x	x	-	-	5-60	x	-

Index of Xenolith Samples (Continued)

Xenolith Lithology	Sample No.	whole rock chemistry and normative mineralogy	thin section	electron microprobe analysis		petrographic description (page #)	hand specimen photograph	photomicrograph (page #)
				plagioclase	mafic min.			
<u>CIPW Silica Oversaturated</u>								
alkali granite	N-7(6)-17	x	x	x	-	5-55	x	-
alkali granite	CC-1	x	x	-	-	5-54	x	-
gneiss	NE-81-V-1	x	x	-	-	5-57	x	-
<u>No Whole Rock Data</u>								
chromitite	CB-AD-8530	-	x	-	x	5-37	x	157
granular amphibolite	N-81-111	-	x	-	-	5-47	x	-
mixed:gabbro (2/3)/ diabase (1/3)	N-81-257	-	x	x	x	5-18	x	-
gabbroic anorthosite	N-81-106	-	x	x	-	5-10	x	-
amphibole in feldspar and quartz groundmass	N-8400-A3	-	x	-	x	5-52	x	-
garnet	S-116	-	x	-	x	5-62	x	-
plagioclase gneiss	N-81-159	-	x	x	x	5-58	x	-

plagioclase schist) are marked \oplus , a trachytic-textured altered diabase is marked \boxtimes , and two green-colored highly saussuritized plagioclase bearing xenoliths are marked \oplus .

To give the reader a general feeling for the whole rock compositions in terms of the mineral phases present, an example is discussed here. Average measured plagioclase compositions for the three troctolites (\square) in the lower left hand corner of the field (Figure 30) were An79, 80, and 82 (by electron microprobe, Appendix 4-C). Average measured plagioclase compositions for the two gabbroic anorthosites (\circ) plotting above 3 wt. % total alkalis were An63 and An69 as noted.

The two green saussuritized plagioclase xenoliths (\oplus) are higher in total alkalis than the remainder of the suite, but measured plagioclase compositions (electron microprobe) in these two xenoliths were extremely variable, with each specimen having a range in An content of about 30 mole % (see legend accompanying Figure 35, p.138).

Figure 31 (p. 124) shows a KCN diagram. The xenoliths are all high (≥ 0.8 normalized weight proportion) in the CaO component, except for the two granites (CC-1 and N-7(6)-17), the gneiss (NE-81-V-1), and the two green saussuritized plagioclase xenoliths (\oplus) as discussed above. The three most sodic gabbroic anorthosites fell below the 0.8 CaO proportion line and had measured (electron microprobe) plagioclase compositions of An 62, 62, and 69.

Figure 29. Total alkali versus silica diagram.

Compositions of xenoliths from this study plot in the diagonal-lined field, except as noted for granites (⊙ CC-1 and N-7(6)-17), gneiss (□ NE-81-V-1) and altered ultramafic (★ 13-81-227).

Outlined field boundaries are highly generalized limits of variability for the lithologies shown, taken from LeMaitre (1976).

Approximate regions for nepheline syenites (high alkali) and granites (high silica) are noted for comparison.

Boundary between alkali and tholeiitic compositions after MacDonald and Katsura (1964).

Figure 30 . Whole rock total alkali versus silica diagram for analyzed xenoliths.

Note the designation of the approximate SiO_2 limits for basic and ultrabasic rocks (1981 AGI glossary), and the line of demarcation between alkali and tholeiitic compositional fields (MacDonald and Katsura, 1964).

Sample key (lithologic names assigned according to discussion p. 165).

- anorthosite
- gabbroic anorthosite
- ▽ gabbro
- △ norite
- + gabbronorite
- troctolite
- * mottled ultramafic/mafic rocks
- ⊕ green saussuritized plagioclase
- ⊖ mafic amphibolites (including granular amphibolites and amphibole-plagioclase schist)
- ⊗ diabase

(See Table 8, p. 19 for listing and lithologies of analyzed samples)

"An" contents marked on diagram denote measured An mole % (electron microprobe) for some low and high total alkali samples to aid in comparison with bulk rock chemistry shown here.

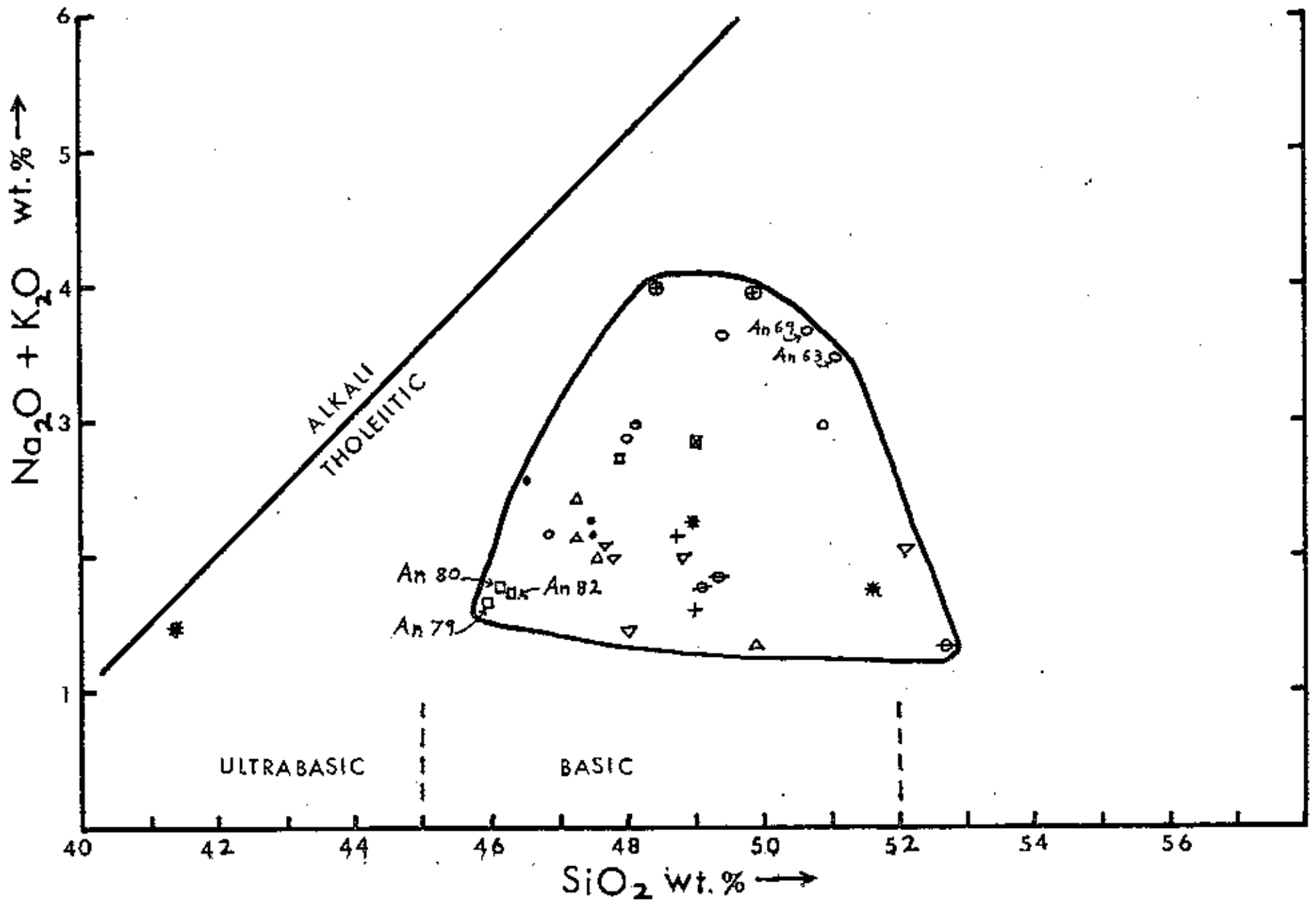


Figure 31. KCN Diagram (Wt.% oxides, normalized to 100%: $\text{Na}_2\text{O} = \text{Na}_2\text{O}/(\text{Na}_2\text{O} + \text{K}_2\text{O} + \text{CaO}) \times 100$, etc.)

Two granites (CC-1 and N-7(6)-17) and a gneiss (NE-81-V-1) plot toward alkaline side of diagram.

Majority of xenolith samples are high in CaO component. (≥ 0.80 CaO proportion line is marked).

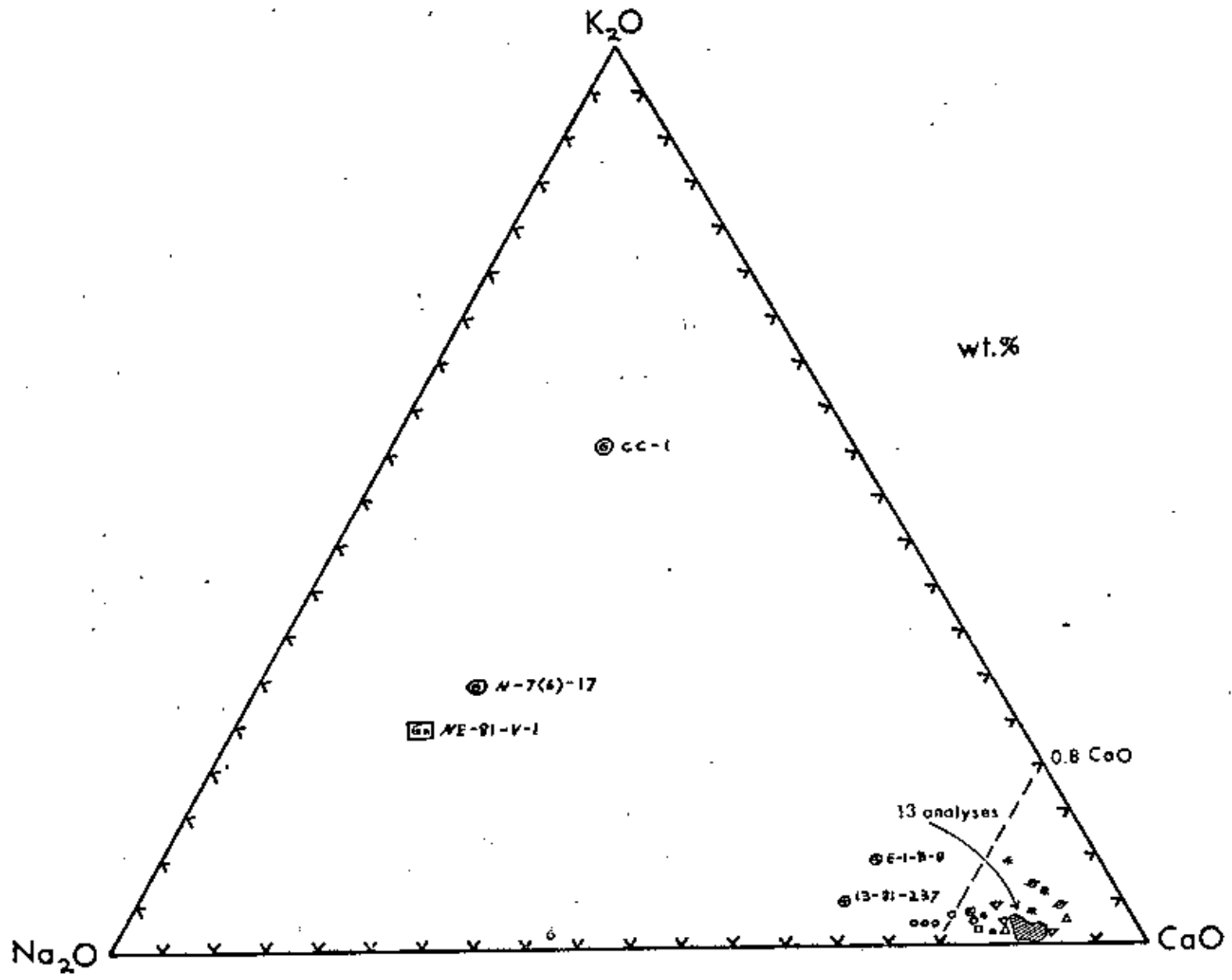
Green saussuritized plagioclase xenoliths (\oplus) E-1-B-8 and 13-81-237 are labeled.

The three most sodic gabbroic anorthosites (000) have measured plagioclase compositions (electron microprobe) of An 62, 62, and 69.

The diagonal-lined field represents 13 tightly clustered analysis

Sample key:

- anorthosite
- gabbroic anorthosite
- ▽ gabbro
- △ norite
- + gabbronorite
- troctolite
- * mottled ultramafic/mafic rocks
- ⊕ green saussuritized plagioclase
- ⊖ mafic amphibolites (including granular amphibolites and amphibole plagioclase schist)
- ▣ diabase
- ⊙ granite
- ⊞ gneiss



In general, the low to moderate silica contents (Figure 30) and the large CaO component reflect the basic overall composition of the xenoliths (excepting the two granites and the gneiss).

Figure 32 (p. 126) shows an FMA diagram. The plagioclase-rich anorthosites and gabbroic anorthosites plot toward the A ($=\text{Na}_2\text{O} + \text{K}_2\text{O}$) corner, which is a reflection of the low mafic mineral content of these samples. (Recall, however, from Figure 31 that these samples are still high in the CaO component relative to Na_2O and K_2O , and should not be viewed as alkali "rich".) The two most iron-enriched samples are the green saussuritized plagioclase xenoliths (\oplus -E-1-B-8 and 13-81-237. The two granitic and one gneissic xenoliths are not plotted on this diagram.

Minor Oxides

P_2O_5 ranges from 0.00 - 0.06 wt. % in the xenolith samples, except for Samples E-1-B-8 (0.13 wt. % P_2O_5) and 13-81-237 (0.11 wt. % P_2O_5), both green saussuritized plagioclase-rich xenoliths, which are enriched above the group..

TiO_2 ranges from 0.05 - 0.44 wt. %, except for Samples E-1-B-8 (1.15 wt. % TiO_2) and 13-81-237 (0.97 wt. % TiO_2) which are enriched above this group. Both of these samples are green saussuritized plagioclase-rich xenoliths.

Figure 32.

F M A diagram (weight % oxides,
normalized to 100%)

Sample key symbols as in Figure 31,
p. 124.

Most samples are enriched in
MgO relative to $(\text{FeO} + \text{Fe}_2\text{O}_3)$
except for two green saussuritized
plagioclase xenoliths \oplus , and
a diabase \boxtimes .

Plagioclase-rich xenoliths with
low mafic mineral contents plot
toward alkali corner.

Trace Elements

Trace element concentrations for the xenoliths are listed in Appendix 2. The distributions for vanadium and nickel are depicted in Figure 33 (p.128).

Vanadium content exhibited a fairly continuous distribution from 1 - 96 ppm. The two green saussuritized plagioclase samples E-1-B-8 (199 ppm V) and 13-81-237 (221 ppm V), and a diabase WCB-1 (221 ppm V) fell outside the above range. Both E-1-B-8 and 13-81-237 contained abundant minute opaque oxides (pp. 5-43, 5-44), and the V may have been localized in these grains. These oxides in sample E-1-B-8 were determined to be titaniferous magnetite by electron probe analysis (Appendix 4-G).

Nickel ranges from 15-594 ppm in the xenolith samples, except for the two granites and one gneiss (0 ppm), and one ultramafic sample (13-81-227 = 903 ppm Ni). This sample contains relict olivine and the high Ni content may represent an original high olivine content in the rock.

Cox, et al., 1979. (p. 334, Table 14.1) give a distribution coefficient of $K_D=10$ for Ni in olivine relative to a basaltic melt. While this number is highly variable, in general the K_D for Ni in olivine is higher than the K_D for Ni in the other common mafic minerals (orthopyroxene, $K_D \approx 4$; clinopyroxene, $K_D \approx 2$;

Figure 33. Histogram of V (top) and Ni
(bottom) distribution in
xenolith samples.
(See text p. 127)

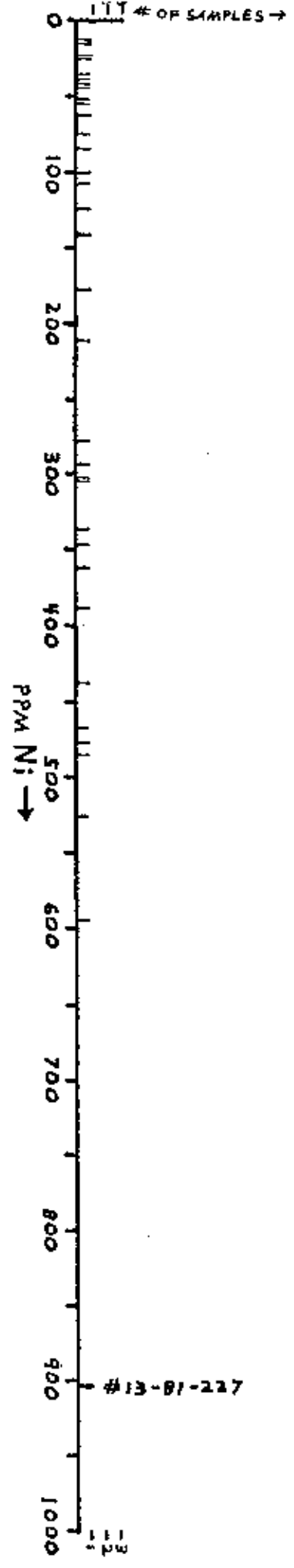
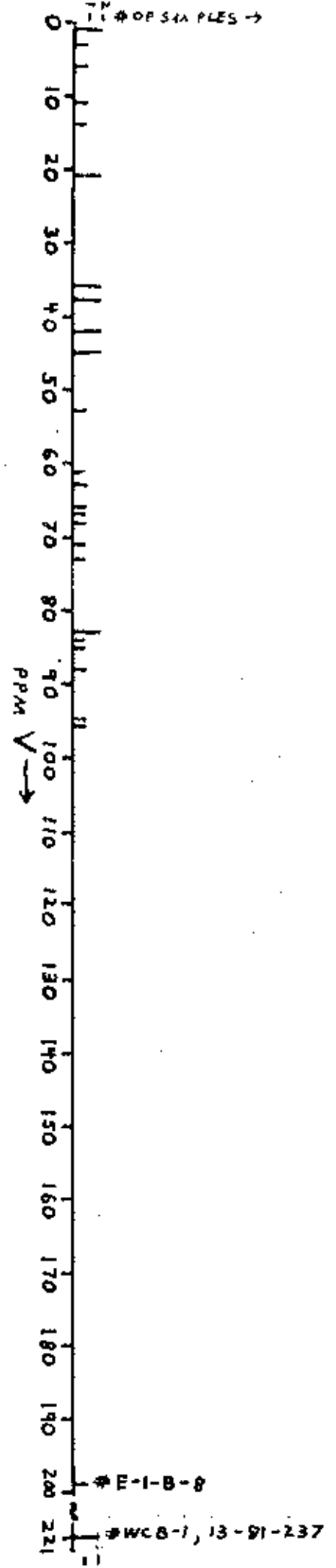


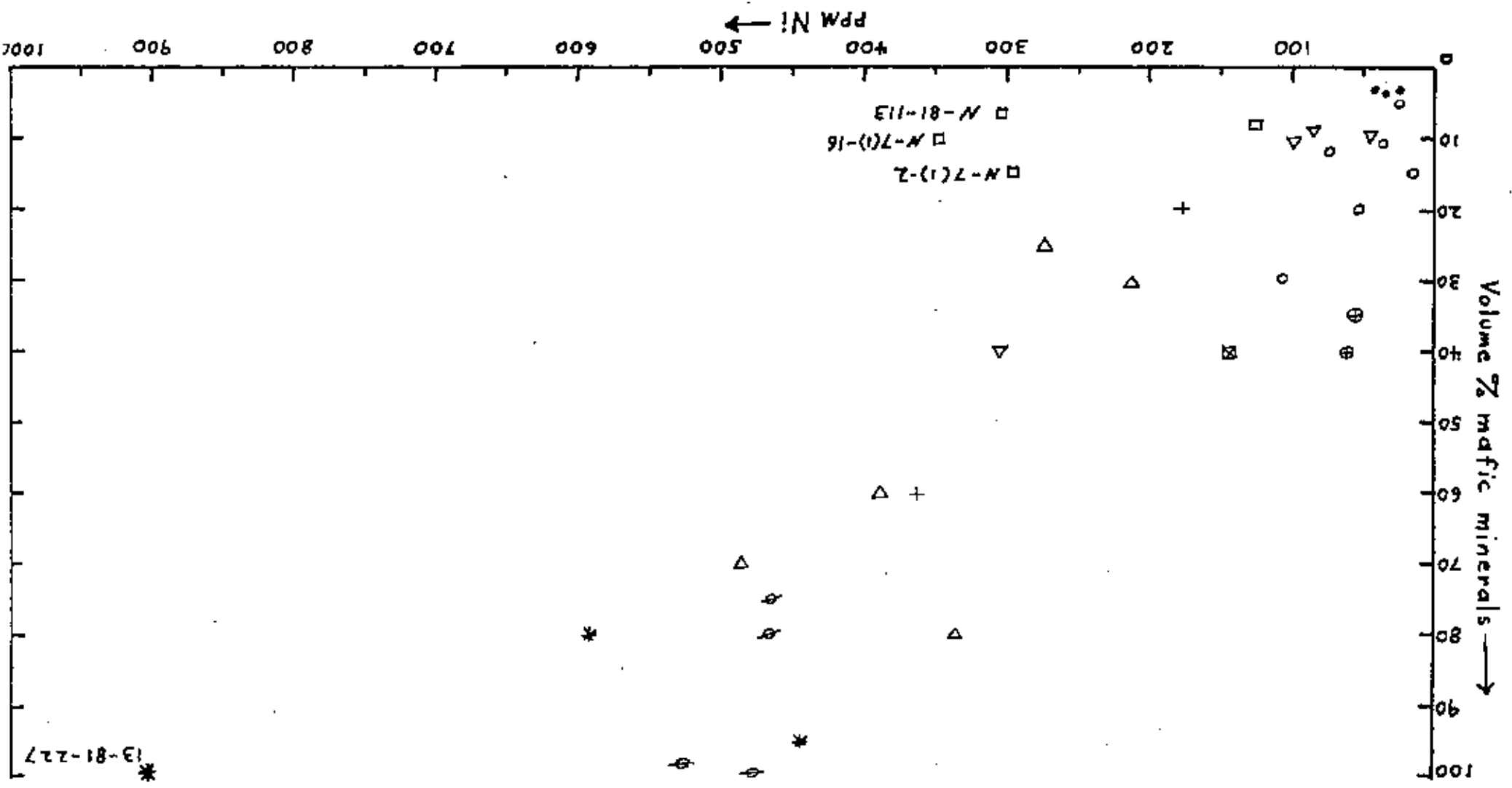
Figure 34. Plot of volume % mafic minerals versus whole rock Ni ppm for xenoliths.

Sample 13-81-227 has remnants of olivine visible in thin section.

Sample N-7(1)-2, N-7(1)-16, and N-81-113 are low in mafic mineral content but have relatively high Ni contents.

Samples CC-1, N-7(6)-17 (granites), and NE-81-V-1 (gneiss) not plotted. All three = 0 ppm Ni.

Sample key symbols as in figure 31 p. 124..



amphibole, $K_D \approx 3$), and 3 orders of magnitude higher than the K_D for Ni in plagioclase ($K_D \approx 0.01$). Figure 34 shows that a rough correlation exists between the percentage of mafic minerals in the xenoliths and the Ni content (p.129).

Three samples, N-7(1)-2, N-7(1)-16, and N-81-113, showed relatively high Ni contents (292-348 ppm) relative to the small amount of mafic minerals (8-15%) they contained. These samples were classified as troctolites (plagioclase-olivine cumulates) based on textural and mineralogical evidence (p.166), and the high Ni contents may provide additional evidence for original olivine (now altered) in them.

Relative Element Gain/Loss Between Interior and Exterior of Xenoliths

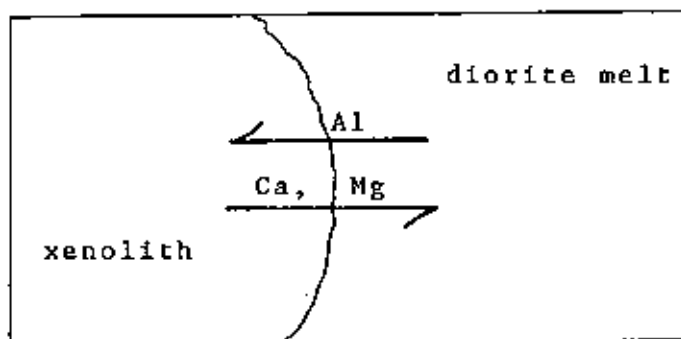
A comparison of the whole rock chemistry of the interior (core) and exterior (material from the outer 1 cm thickness of xenolith) was made for each of two large cumulate textured xenoliths, a gabbro (NE-81-245) and a mafic gabbro (NE-81-244). Both xenoliths were approximately 31 cm long in their longest dimension (discussed on pp. 92-93 ; Figure 25, p. 100; and pp. 5-17 and 5-21).

Appendix 1-C compares the relative element gains and losses. A positive residual (App. 1-C) for an element as used here means that analysis showed a gain in that element going from the interior of the xenolith to the exterior of the xenolith (i.e., the exterior rim was enriched relative to the interior for that element).

A "significant" gain/loss is defined here as a gain/loss for any element which is greater than two times the average analytical error (Table 2, p. 27) for that element (i.e., gain or loss $> 2 \cdot$ (analytical error)).

Aluminum showed a significant enrichment in both xenoliths in the exterior rims (avg. = +2.02 wt.% as Al_2O_3). Elements showing a significant depletion in the exterior rims of both xenoliths were Mg (avg. = -1.96 wt.% as MgO) and Ca (avg. = -0.67 wt. % as CaO).

Upon heating of the xenoliths in the host diorite melt which formed the central Lodgepole Intrusion, the relative movement of elements can be schematically represented as:



The calcium and magnesium loss from the xenolith exterior appears to represent diffusion of these elements toward the diorite melt, which had a lesser concentration of these elements. (The fine-grained diorite (Appendix 1-A) was lower in Ca and Mg than either the two cumulate-textured xenoliths, NE-81-244 or NE-81-245). The aluminum gain appears at first to be against the whole-rock chemical gradient (i.e., the plagioclase-rich xenoliths are higher in Al than the fine-grained diorite (compare Appendices 1-A and 1-C). However, the plagioclase in these xenoliths was relatively unaltered by metamorphism in the diorite melt (as discussed on p.164) and the Al enrichment of the xenolith rims may have been due to Al enrichment of the originally low-Al mafic minerals (clinopyroxene) in the xenoliths by fluids from the diorite melt. The increase toward the xenolith rims in the Al content of metamorphic amphiboles in the xenoliths (Figure 38, p. 147) provides additional evidence for the addition of Al to the xenoliths from the melt. (See p.160 for a discussion of the composition of reaction rims on the xenoliths).

Loss on Ignition

The Loss on Ignition (LOI) at 900° C (see Appendix 6 for procedure) for xenolith samples is tabulated in Appendix 1. LOI (at 900° C) ranged from an average of

1.43 wt.% (for the three anorthosites) to 3.75 wt. % (13-81-227, altered ultramafic), 3.85 wt. % (N-81-162, altered gabbro-norite with 60% mafic minerals), and 5.75 wt.% (TR-1(0)-1, altered ultramafic rock) for some dominantly mafic samples. The bulk of the mafic minerals in these xenoliths consisted of calcic amphiboles (tremolite-actinolite, and hornblende) (p. 143), with some chlorite (p. 150). These minerals are hydrous silicates, with one-atmosphere dehydration temperatures below 900° C (Deer et al., 1977, p. 164 - tremolite, p. 170 - hornblende, p. 236 - chlorite), and were the likely major source of water-loss in the LOI determinations.

Normative Mineralogy

The CIPW normative mineralogies for the xenoliths were calculated from whole rock chemical analysis using the RKNORM Program (Dr. Peter Wiegand, California State Northridge). Normative mineralogies for the xenoliths are tabulated in Appendix 3. The ferromagnesian minerals in Appendix 3 are listed in terms of hypersthene, augite, and olivine, with the MgO/FeO ratio of each of these minerals expressed by the mole fraction MgO. Because measured Fe₂O₃/FeO ratios were highly variable in the xenoliths (0.41 — 3.08; avg. = 0.74 by weight), a ratio standardized at Fe₂O₃/FeO = 0.15 by weight (listed in Appendix 1-D) was used in the normative calculations, as suggested by Cox et al. (1979, p. 412).

The majority of the xenoliths are silica saturated igneous rocks (hypersthene and olivine normative). Three specimens of granitic composition are oversaturated (quartz normative). One ultrabasic sample (13-81-227) and three anorthositic samples were marginally silica undersaturated (2.51 — 0.02 normative wt.% nepheline).

Mineral Textures

The words cumulus and intercumulus are used in this text according to the criteria defined by Jackson (1967). A summary of these criteria follows here.

Cumulus crystals are inferred to have been deposited in a magma chamber primarily by gravitative and/or magmatic current deposition. They are distinguished petrographically by tabular, equant, rounded or embayed habit; subhedral to euhedral shape, random orientation or igneous lamination in thin section; and few inclusions of other cumulus minerals.

Intercumulus minerals occur as oikocrysts and space fillings between cumulus grains, are anhedral in shape, show a limited number of crystallographic directions in a single thin section, and may have abundant inclusions of cumulus minerals.

In the cumulate textured xenoliths examined in this study, plagioclase occurs as an unaltered primary cumulus mineral. Primary igneous ferromagnesian minerals did not occur in the xenoliths as cumulus phases, these having been metamorphically altered to crystal aggregates of actinolitic-tremolitic to hornblendic amphiboles and chlorite. The euhedral to subhedral external shape and tabular to rounded external habit of these metamorphic mineral domains, the presence of relict cleavage in these metamorphic assemblages, and the occurrence of these mafic

domains in plutonic igneous rocks of basic composition provide evidence for their original cumulus nature.

(See photomicrographs, Figures 39, p. 148; 41, p. 151; 42, p. 152; and 44, p. 155.)

Chromite occurs as a cumulus phase in one sample (CB-AD-8530).

Augite occurred as an intercumulus mineral between cumulus plagioclase grains in some xenoliths where it was apparently protected from metamorphic fluids. Actinolitic-tremolitic to hornblendic amphibole occurred as anhedral shaped crystal aggregates between cumulus plagioclases, and in some thin sections occurred as an alteration product around the periphery of primary intercumulus augite.

Mineralogy - Cumulate Textured Xenoliths

The mineralogy of the cumulate textured basic xenoliths (p. 5-1 - 5-44 , Appendix 5) is reviewed here.

Plagioclase

Compositions determined by electron microprobe for cumulate textured plagioclase in the xenolith samples are listed in Appendix 4-C. Figure 35 shows a histogram of average plagioclase compositions (An mole %) as taken from Appendix 4-C, (p. 138).

Measured sample average compositions (rounded to whole numbers) ranged from An62 to An86. In general, the total composition range among a series of individual analyses in a given sample was small (0.25 -- 5.16 mole % An) for the samples in Appendix 4-C. Exceptions to the above per sample An (mole %) range were: NE-81-245QUT (11.72 An range), NE-81-501 (30.90 An range), E-1-B-8 (32.56 An range), and 13-81-237 (27.91 An range).

Grain sizes for the cumulate textured, euhedral to subhedral, equant to tabular plagioclase crystals were in the 1 - 7 mm range. One specimen (gabbroic anorthosite, N-81-8720-A3, p. 5-13) had noticeably larger (10-15 mm) euhedral, tabular plagioclase crystals.

Plagioclase compositions for each sample are also noted along with the petrographic descriptions in Appendix 5.

Figure 35. Histogram of average plagioclase compositions for plagioclase cumulate samples (Compositions determined by electron microprobe, listed in Appendix 4-C).

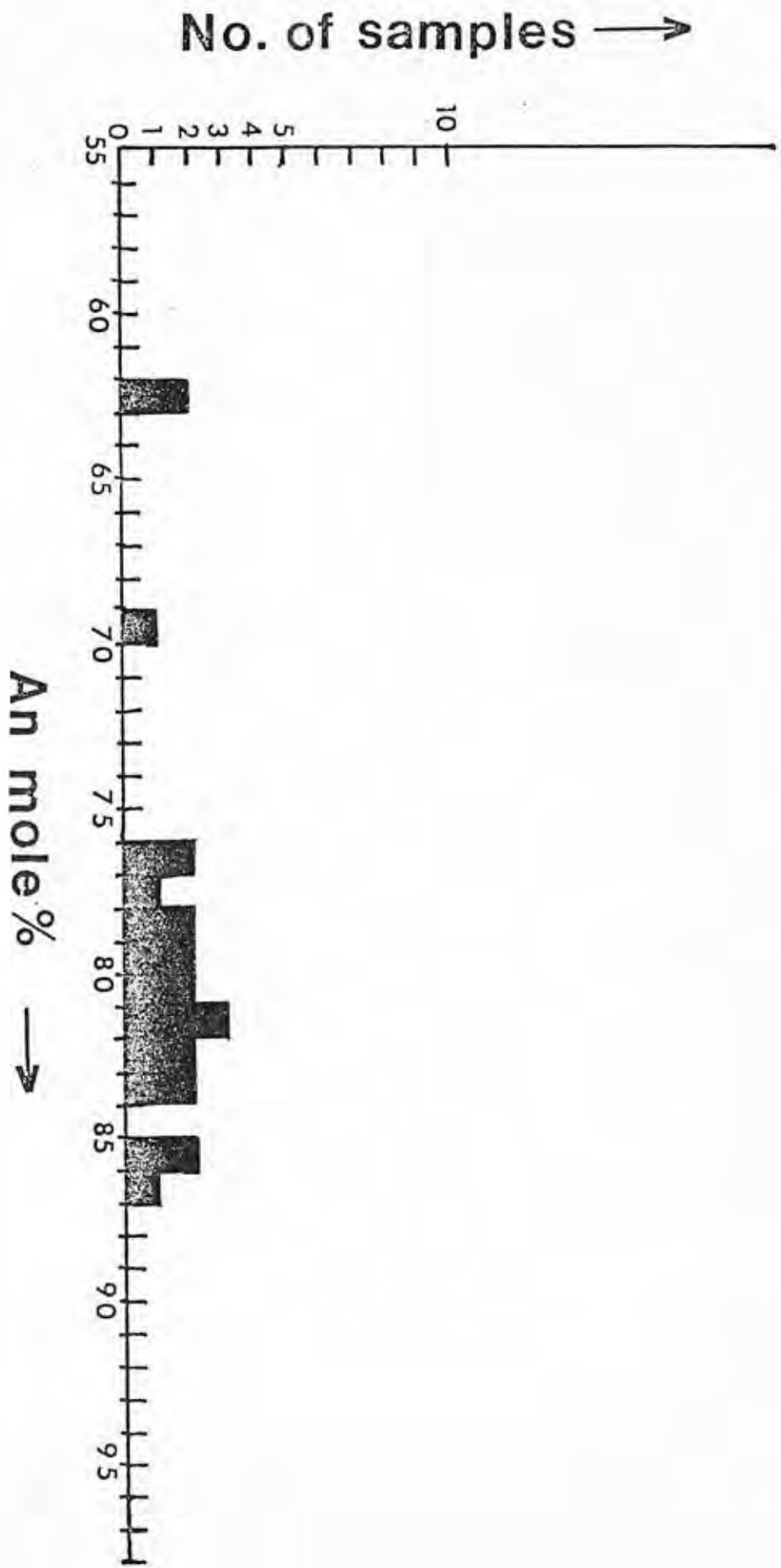
Note:

(1) each sample is plotted as a unit block (■) between the two whole An mole %'s where its average composition lies.

(2) the average An of the two samples (NE-81-244IN and NE-81-244OUT), and the average An of the two samples (NE-81-245IN and NE-81-245OUT) were each plotted as a unit block, because each set of IN/OUT samples represented two thin sections from the same sample.

(3) Samples NE-81-501 (An 78.64, range in An = 30.90), E-1-B-8 (An 78.12, range in An = 32.56), and 13-81-237 (An 47.28, range in An = 27.91) were not plotted because of the extreme sample variability in plagioclase compositions.

(4) Samples N-81-159 (An 36.44, plagioclase gneiss, p. 5-58) and N-7(6)-17 (An 16.80, alkali granite, p. 5-55) are not plotted.



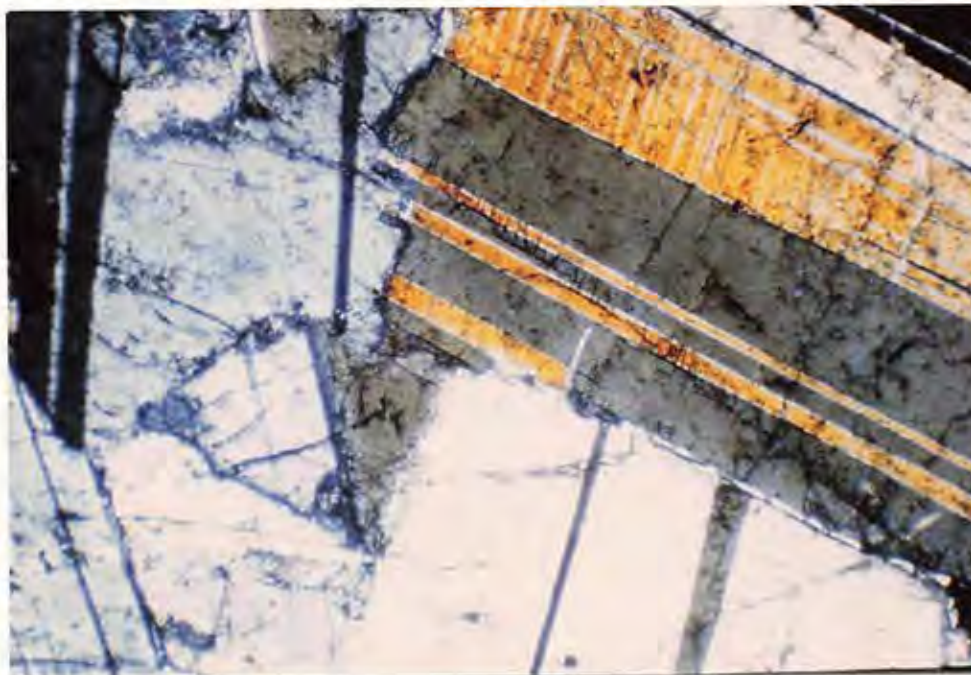


Figure 36. Sample # 13-81-229 (page 5-3)

(crossed nicols; field of view 5 mm left to right). Extreme adcumulus*texture in anorthosite. Tabular bytownite (An 82). Intercumulus clinopyroxene in the sample (not visible) had a composition of Ca₄₅ Mg₄₂ Fe₁₃(mole prop.)

This texture was common in the specimens classified as anorthosites in Appendix 5.

* an adcumulus rock, as defined by Wager and Brown (1967, p. 65), is one in which originally settled crystals have been enlarged by growth of the same mineral after initial crystal settling. Post-settling enlargement of cumulus crystals is necessary because originally settled crystals must obviously have some pore space. Wager and Brown (1967, p. 64-66) estimated initial pore space at $\approx 40\%$ using simple tabular-shaped pellet settling experiments.

One altered ultramafic sample (N-81-161, p. 5-39) had minor amounts of anhedral, 1 — 2 mm plagioclase (possibly intercumulus), as did a mafic gabbro (N-81-203, p.5-22).

Augite (Ca, Mg, Fe, Na, Mn, Al)₂ (Si, Al)₂O₆

Augite occurred in the cumulate textured xenoliths as intercumulus anhedral space fillings between plagioclase grains in some of the more anorthositic specimens. Augite was not preserved in the more mafic specimens.

Electron microprobe analysis of augites are listed in Appendix 4-D. Table 9 (p.141) lists the Ca-Mg-Fe atomic % of measured augite grains.

The augite was very pale green-brown to pale green to nearly colorless in thin section, and was non-pleochroic. An example is shown in the photomicrograph of Figure 37 (p.142.)

Some augite grains were partially altered to calcic amphibole (tremolite-actinolite and/or hornblende) along grain boundaries. The higher Al content and lower Ca content of these calcic amphiboles (see electron probe analysis, Appendix 4-D) compared to the augite supports the observation, mentioned on p. 131 under whole rock chemistry, that the xenolith rims gained Al and lost Ca upon undergoing metamorphism. The overall abundance of

Table 9. Clinopyroxene (Augite) Compositions Measured by Electron Microprobe (Whole-mineral analysis in Appendix 4-D).

All of these grains occurred as anhedral, intercumulus minerals interstitial to cumulate textured plagioclase, except as noted.

Sample #	Page listed in Appendix 5	Mole Proportions		
		Ca	Mg	Fe
13-81-229	5-3	45	42	13
N-81-502	5-25	48	48	4
N-7(1)-2	5-32	46	45	9
N-81-113	5-33	46	44	10
N-81-159*	5-58	42	41	17

* occurs as 1 mm granoblastic crystals within 15 mm mafic aggregates in a feldspar (An36) - quartz gneiss.

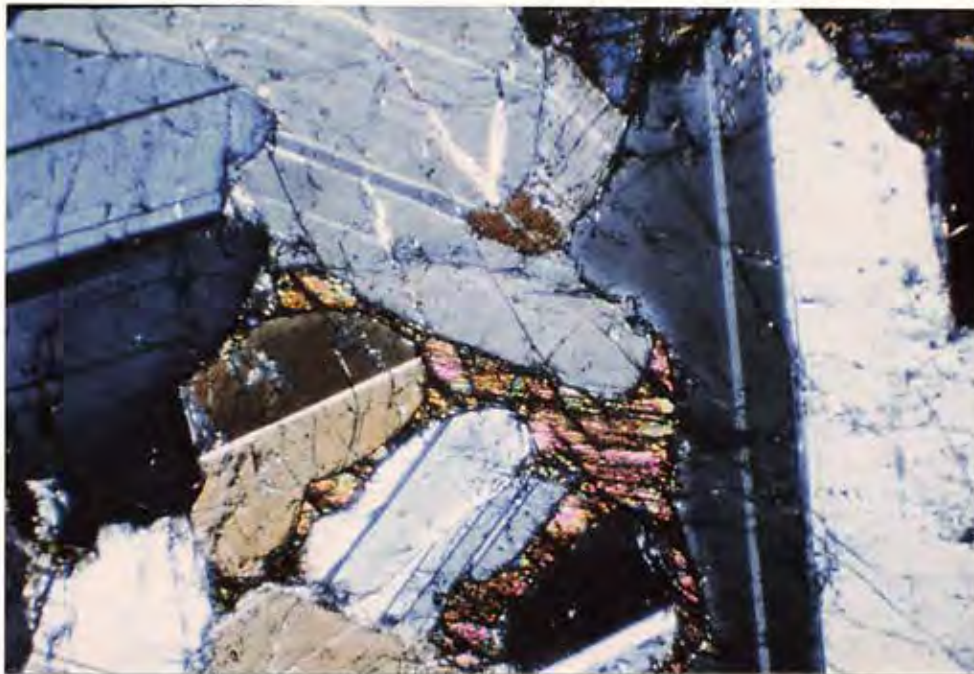


Figure 37. Sample # N-81-113 (page 5-33)

(Crossed nicols, field of view of 5 mm, left to right). Cumulus textured plagioclase (An82), with intercumulus anhedral augite of composition $\text{Ca}_{46} \text{Mg}_{44} \text{Fe}_{10}$ (mole prop.) (center, and top right). This texture was common in the anorthosites and gabbroic anorthosites in Appendix 5. In some cases, the augite could be seen partially altered to light green actinolite along cleavage and fractures.

preserved augite in the xenoliths was not possible to determine due to the difficulty of distinguishing it from these light green amphiboles in hand specimen.

Deer et al. (1977) state that "augite is frequently altered to a uraltitic amphibole, either as a single crystal or as an aggregate of small prismatic crystals. The alteration usually begins at the periphery or along the cleavages" (ibid., p. 128). "In many basic rocks, pyroxene is altered marginally to a pale green amphibole to which the name uralite is given. This amphibole is considered to be actinolitic in composition" (ibid., p. 166).

Because no preserved cumulate textured augite was encountered, no attempt was made to predict the possible composition of any coexisting orthopyroxene. The augite encountered was intercumulus and its anhedral habit appears to represent crystallization of interstitial trapped liquid.

Tremolite -actinolite and hornblende

The dominant mafic minerals in the cumulate textured xenoliths (and also in the granular amphibolites) were calcic amphiboles of tremolite-actinolite to hornblende compositions.

As used in this study tremolite-actinolite denotes light green, non-to-weakly pleochroic, calcic amphiboles

of the series $\text{Ca}_2 (\text{Mg}, \text{Fe}^{+2})_5 (\text{Si}_8\text{O}_{22}) (\text{OH})_2$, (Deer et al., 1977).

The term "tremolite" was used only when the amphibole was very light green and non-pleochroic. Electron probe analysis determined that these non-pleochroic amphiboles had a ratio $\text{Mg}/(\text{Mg} + \text{Fe} + \text{Mn}) > 0.8$ (Appendix 4D), placing them in the tremolite portion of the series (Deer et al., 1977, p. 164, Fig. 59). Weakly pleochroic light green actinolite had higher Fe contents.

With increasing Al content and decreasing Si content (Figure 38, p.143), the amphibole became a darker green and strongly pleochroic hornblende series amphibole, $(\text{Na}, \text{K})_{0-1} \text{Ca}_2 (\text{Mg}, \text{Fe}, \text{Al})_5 (\text{Si}_{6-7} \text{Al}_{2-1} \text{O}_{22}) (\text{OH})_2$.

Deer et al., (1977, p. 1163) state that "there is probably a continuous range of compositions between the tremolite-ferroactinolite and the hornblende series; because however of the extremely wide range of composition of the calcium amphiboles it is convenient to consider separately the aluminum-poor tremolite-ferroactinolites. The division between this and the hornblende series is, however, an arbitrary one."

The amphiboles occur in a number of different textural habits:

- (1) granular to blady actinolitic (300-500 μm individual crystals). amphibole occurred as an alteration product of augite along augite grain boundaries.

- (2) granular to blady tremolite-actinolite (300-500 μ m crystals) occurred in anhedral assemblages (up to \approx 3 mm across) between cumulus plagioclase grains. The actinolite commonly is surrounded by thin (< 1 mm) rims of dark green pleochroic hornblende in contact with the plagioclase.
- (3) Tremolite-actinolite series amphibole occurred as parallel-oriented blady crystals (0.2 - 1.0 mm), in subhedral to euhedral, blocky to rounded domains (4-7 mm across). In this paragenesis it is rimmed locally by dark green granular hornblende along the peripheries of the individual tremolite-actinolite domains. (The photomicrograph of Figure 39, p.148 illustrates textural and compositional features which this author interprets to represent tremolite-actinolite pseudomorphic after original clinopyroxene). An example of this texture in hand specimen can be seen in the rounded mafic aggregates of sample CBE-4 (p. 5-16).
- (4) Fine-grained tremolite-actinolite in granular to blady intergrowths occurs as the dominant, or even sole, mafic mineral assemblage in many of the more mafic cumulate textured xenoliths. The actinolite becomes coarser grained, darker green,

strongly pleochroic hornblende toward the exterior of xenoliths (Figure 40, p.149).

- (5) Dark green strongly pleochroic hornblende up to 1 mm in the longest dimension occurs as optically continuous crystals in crack fillings in plagioclases and in interstitial spaces between cumulus plagioclase grains.

Minor amounts (always subordinate to the actinolite) of very fine chlorite flakes occur along with the actinolite and hornblende in the above associations.

Deer et al. (1977, p. 165) state that actinolite, in association with chlorite, is typical of greenschist-facies rocks, and that "in this (greenschist facies) paragenesis it sometimes occurs in parallel intergrowths with hornblende, or in crystals sharply rimmed by hornblende."

In this study, the term "uralite" in Appendix 4-C is reserved for light green to blue green non-pleochroic calcic amphiboles similar in color to the actinolite (i.e., light green color, non-to-very weakly pleochroic) but having a high Al content (>10 wt.% Al_2O_3 by electron probe), and a blocky texture more like the coarser hornblende.

Figure 38. Plot of Al_2O_3 versus SiO_2
(wt.%) for calcic amphiboles
of Appendix 4-D.

+ denote dark green, strongly
pleochroic amphibole,
0 denote light green non-to-
weakly-pleochroic amphibole.
See text, p. 143 for discussion.

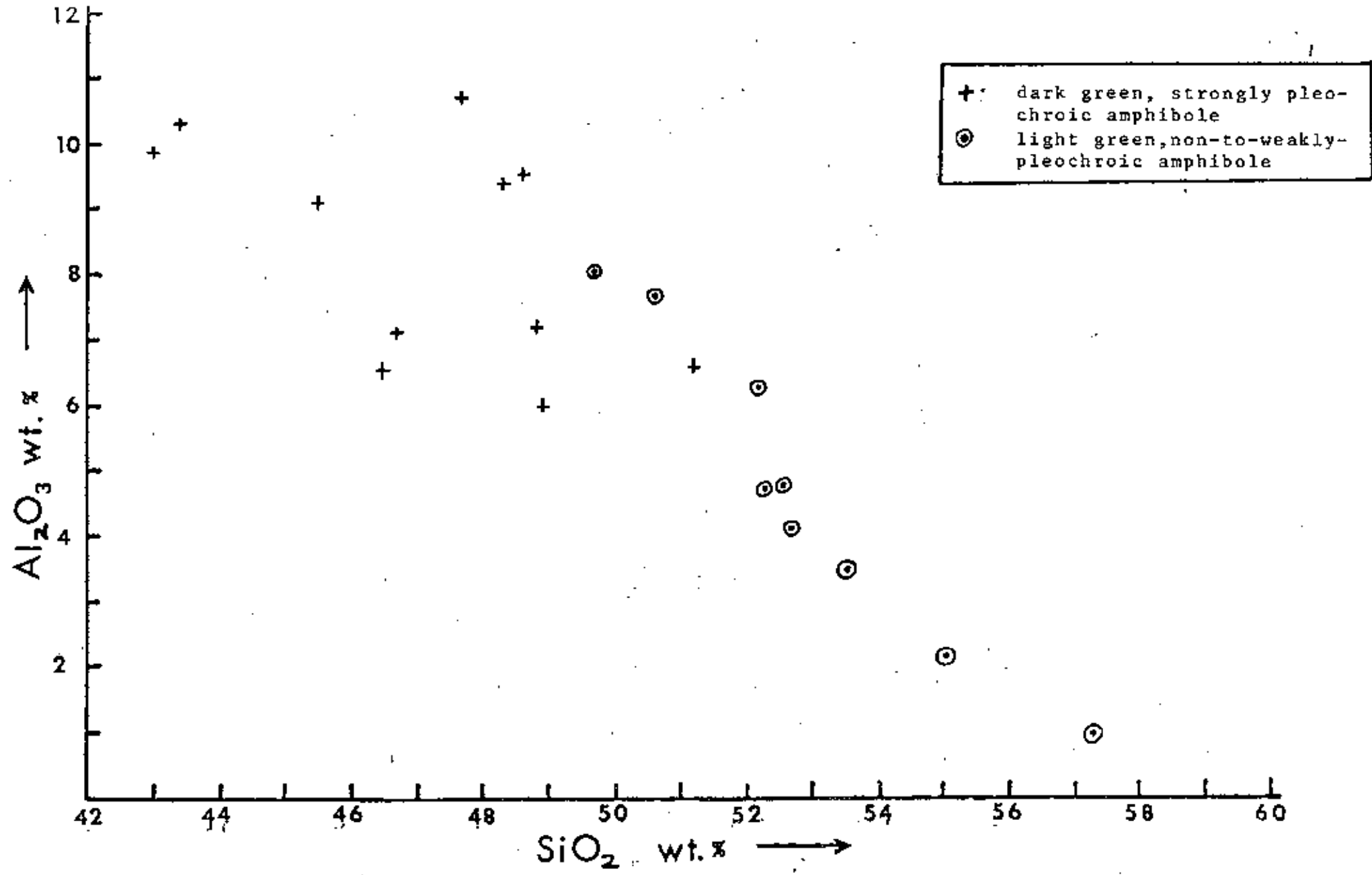


Figure 39. Sample NE-81-501 (p. 5-20)

(Crossed nicols, field of view is 5 mm, left to right). Subhedral domain of tremolite (center) with parallel alignment of blady tremolite within the domain (upper left to lower right striations).

This author believes that tremolite-actinolite occurring in this habit is pseudomorphic after original clinopyroxene for a number of reasons:

- (1) The blocky to rounded outlines of these domains.
- (2) The presence of relict cleavage (upper left to lower right) along which tremolite needles are aligned. This orientation is constant within a domain, but varies between domains (note that the two tremolite domains above the large one in the center have different orientations of the tremolite needles.) This constancy of direction within domains and variation between domains suggests that the growth direction of the tremolite is crystallographically controlled and not controlled by some outside directional stress.
- (3) The occurrence of these tremolite-actinolite domains in augite-normative basic plutonic rocks containing calcic, polysynthetically twinned euhedral plagioclase.
- (4) The high Ca-content of the tremolite-actinolite and other amphiboles in these rocks (see Appendix 4D, tremolite, actinolite, and hornblende analysis).
- (5) The observation that intercumulus augite (see Figure 37) was partially altered to calcic amphibole (tremolite-actinolite and hornblende) in other specimens.

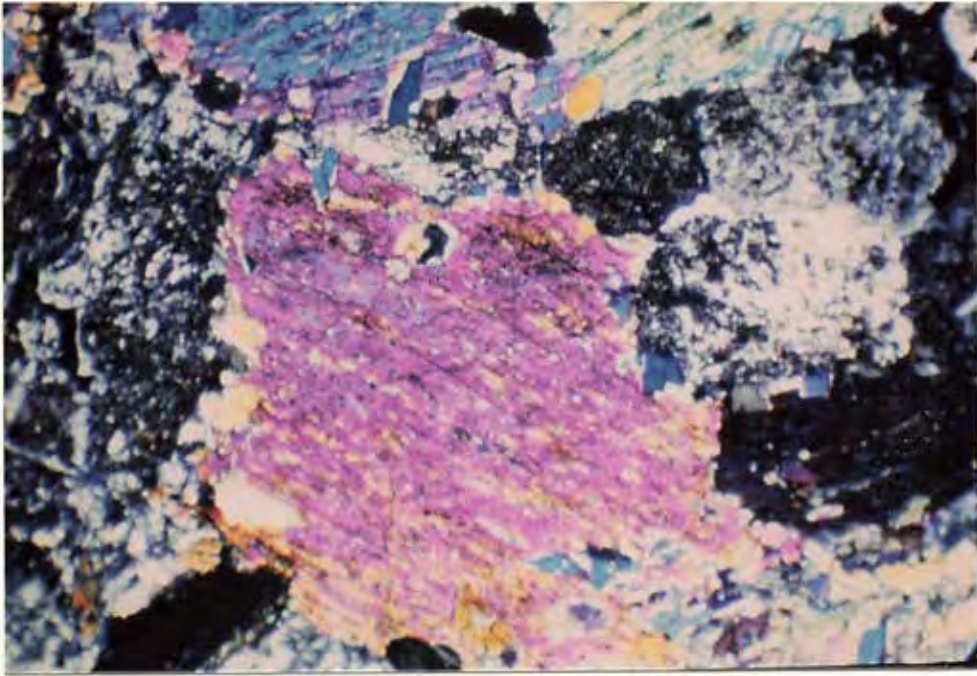


Figure 39.

strongly pleochroic hblde. fine-grained



diorite

light green tremolite-actinolite

1 mm

Figure 40: Photomicrograph of rim on a granular amphibolite xenolith (N-81-8400-A1, p. 5-46). Plane light, scale bar at lower right.

Note, from lower left in photograph to upper right:

lower left-hand half of photograph shows light (light green true color) granular tremolite-actinolite series amphibole, average grain size 300 - 500 μ m. (interior of xenolith).

upper right 1/3 of photograph shows dark (dark green true color) green hornblende which is strongly pleochroic (rim of xenolith), average grain size 500 - 800 μ m.

extreme far right corner is fine-grained diorite host intrusive, which surrounds the xenolith in hand specimen.

The amphibole changes from finer grained light green, non-pleochroic tremolite-actinolite in the xenolith interior to coarser grained dark green, strongly pleochroic hornblende in the exterior rim of the xenolith. Electron microprobe analysis of hornblende and tremolite-actinolite in a variety of the xenoliths has shown that a continuous composition series exists between the higher alumina, lower silica hornblende and the lower alumina, higher silica tremolite-actinolite series (see Figure 38, p. 147).

Chlorite

Chlorite $(\text{Mg,Al,Fe})_{12} ((\text{Si,Al})_8\text{O}_{20}) (\text{OH})_{16}$ occurs in two distinct habits in the xenoliths:

- (1) As small flakes (50 - 100 μm) in associations with randomly oriented granular to blady hornblende and actinolite. In this association it is always subordinate to the amphiboles (generally $< 1/4$ of the mafic assemblage).
- (2) Chlorite occurs in the cores of 3 - 8 mm, rounded to oblate, subhedral mafic domains consisting of large, plate-like crystals of chlorite (2 - 5 mm), surrounded by 1 - 2 mm rims of granular hornblende and/or actinolite. (The photomicrograph of Figure 41, (p.151) illustrates textural and compositional features which this author interprets to represent chlorite pseudomorphic after original orthopyroxene.)

Deer et al. (1977, p. 239) state that chlorite is a common hydrothermal alteration product of pyroxene in igneous rocks, and that "the composition of the chlorite is often related to that of the original igneous mineral".

A chlorite from sample N81-162 had an $\text{Fe}/(\text{Fe} + \text{Mg})$ ratio of 0.21 and a Si content of 6.4 Si per formula unit, placing it in the Mg-rich penninite group (Deer et al., 1977, p. 233, Figure 81).

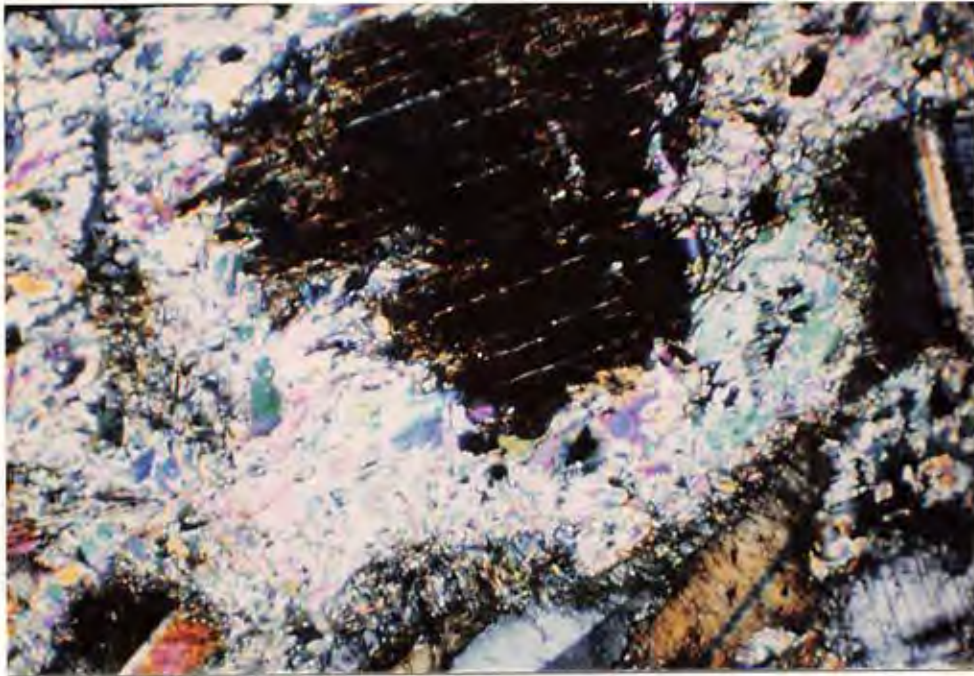


Figure 41. Sample # NE 81-502 (p. 5-25)
 (Crossed nicols, field of view is 5 mm
 left to right). Dark rounded chlorite
 core at top center surrounded by fine
 aggregate of granular actinolite. Poly-
 synthetically twinned subhedral plagioclase
 crystals (An 85) visible at right
 and bottom.

This author believes that a number of factors suggest that chlorite occurring in this habit is pseudomorphic after original cumulus orthopyroxene:

- (1) The euhedral to subhedral, blocky to rounded, shape of the chlorite domains.
- (2) The occurrence of the chlorite in hypersthene normative basic plutonic rocks containing calcic, polysynthetically twinned, euhedral plagioclase.
- (3) The high (Mg + Fe) and low Ca content of the chlorite (see chlorites in Appendix 4-D).

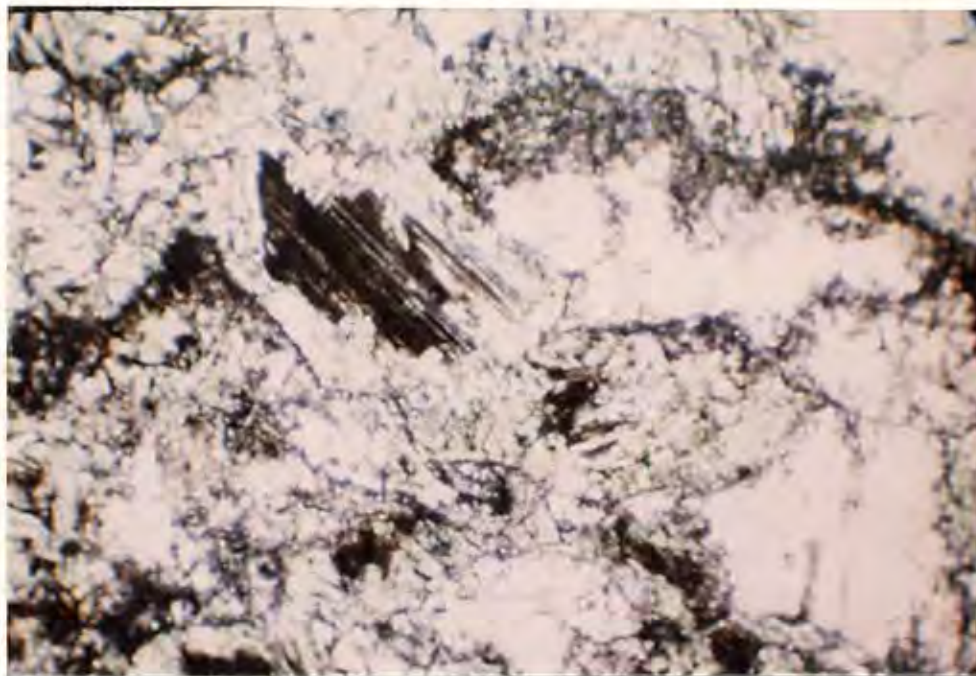


Figure 42. Sample # N81-162 (p. 5-30)
 (Plane polarized light, field of view is
 5 mm, left to right). Light green
 actinolite surrounding dark chlorite core
 (left center). Light green domains
 composed nearly entirely of actinolite
 appear at upper right and right center.
 Note the polygonal, pseudomorphic nature
 of the outlines now filled with actinolite
 and chlorite, or actinolite. White
 areas are plagioclase feldspar.

This author believes that the chlorite
 filled domains are pseudomorphic after
 orthopyroxene and the solid tremolite-
 actinolite domains are pseudomorphic
 after clinopyroxene, for the reasons
 given in the text accompanying Figures
 39 and 41, pp. 148 and 151.

Sample TU-1-80 (p. 5-24) provides an example of the platy chlorite filled mafic areas in hand specimen.

Olivine

Unaltered olivine (Figure 43, p.154) was seen in only one sample (13-81-227, mottled and ultramafic rock, P. 5-41). The olivine composition was not determined.

Evidence for the original existence of olivine in some other xenoliths is by analogy with textural features and alteration products of olivine observed elsewhere in rocks of similar composition (described in the following pages).

Alteration assemblages rimmed by amphibole, with interiors of fine-grained magnetite and chlorite occur as discrete rounded, embayed domains in some cumulus plagioclase rich xenoliths. (An79-82 plagioclase by electron probe, pp. 5-32 to 5-35). These alteration assemblages are magnetic enough to attract a hand-held "pencil" magnet (Figure 44, p. 155).

Raedeke (1979, p. 52) describes olivine altered to serpentine + talc + magnetite in troctolites of similar composition (plagioclase-olivine cumulates) in the Middle Banded Zone of the Stillwater Complex. This author (pointed out by D. P. Gold, Pers. comm.) observed that troctolites of the Stillwater Complex had olivines wholly or partially altered to magnetic assemblages of magnetite and micaceous minerals. Relatively unaltered olivines

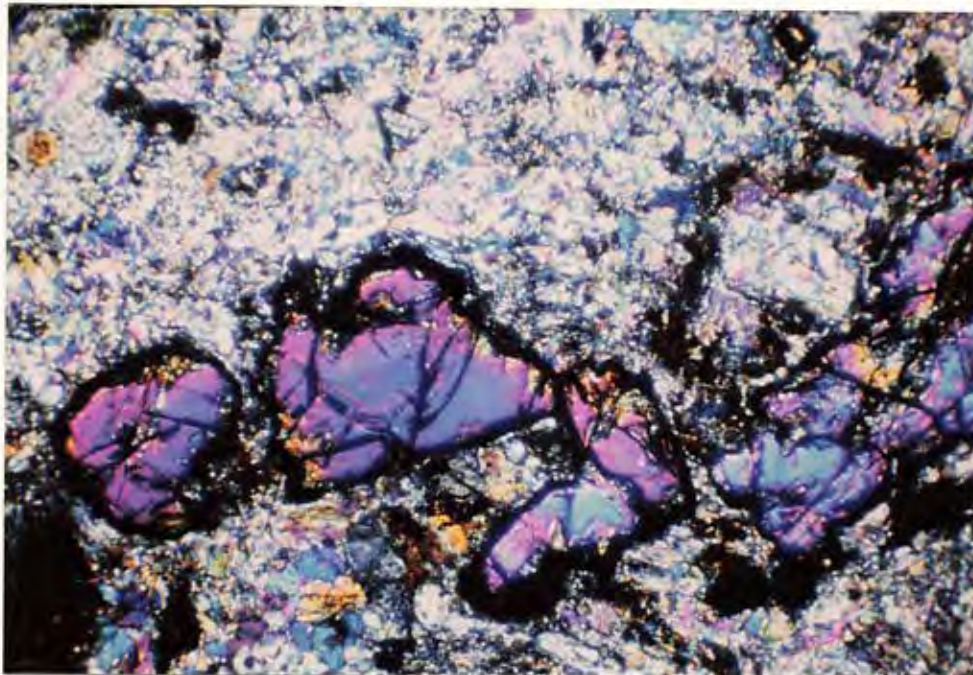


Figure 43. Sample # 13-81-227 (page 5-41)
(Crossed nicols, field of view is 5 mm,
left to right)

Relict olivine (large, high relief grains) in matrix of granular tremolite. This is the only specimen of those listed in Appendix 5 which contained fresh olivine. The random orientation of the tremolite fabric suggests crystallization under isotropic (hydrostatic) conditions.

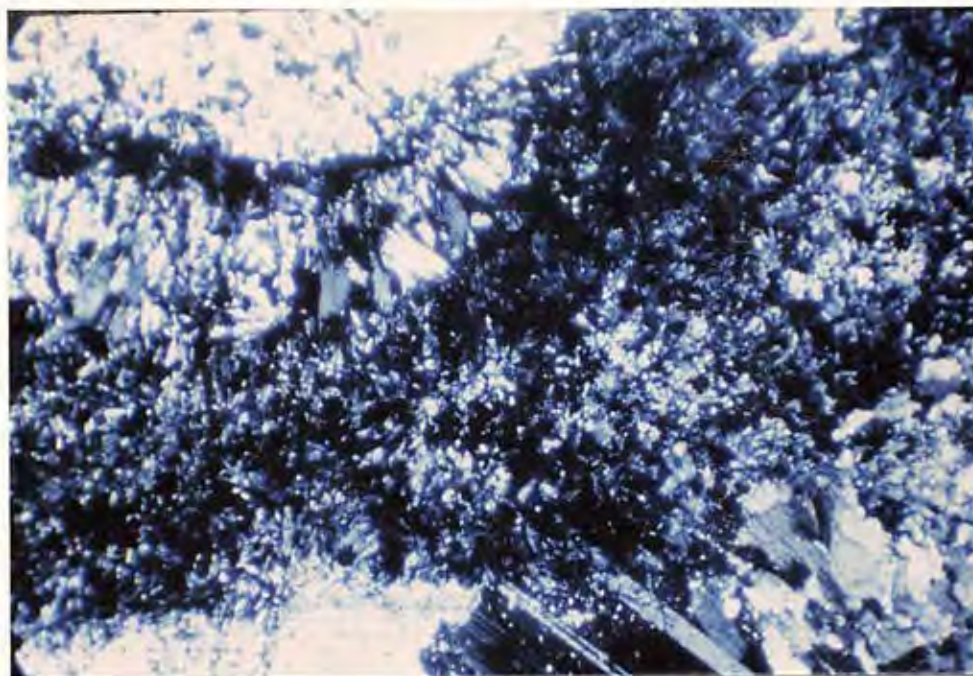


Figure 44. Sample # N-7(1)-16 (p. 5-35)

(Plane polarized light, field of view is 5 mm left to right). Photomicrograph shows a portion of large rimmed alteration assemblage. Polysynthetically twinned plagioclase (An 79) at extreme bottom surrounds rounded and embayed 7 - 8 mm alteration assemblages. Only a portion of one of these assemblages is seen here, showing a dark outer rim (across center of photograph) consisting of chlorite and magnetite and actinolite and a lighter color actinolite area (in center to upper left of photograph) toward core of assemblage.

(See text, p. 153)

are commonly rounded and embayed, and rimmed by a reaction corona of pyroxene, indicating partial resorption of early-formed olivine.

Deer et al. (1977, p. 5) point out that olivine is susceptible to hydrothermal alteration and the effects of low-grade metamorphism, and list fine-grained mixtures of chlorite, iron oxides, and amphibole as possible alteration products, with coronas of amphibole and spinels surrounding olivines in metamorphosed basic rocks.

Chromite

Cumulus textured, euhedral to subhedral chromite, with a grain size of 0.2 - 1.0 mm was found constituting approximately 30% of one xenolith (CB-AD-8530, p. 5-37). Chromite grains analyzed (electron microprobe) had an average composition of 50.16 wt.% Cr₂O₃ (34.32 wt. % Cr), and were unzoned. (Figure 45, p. 157).

(Duke (1983) characterizes chromitites from stratiform bodies as being composed of fine grained (<1 mm) cumulus chromite with interstitial olivine, orthopyroxene, plagioclase and/or clinopyroxene or their alteration products. He characterizes the chromite grain shape as euhedral to subhedral, as opposed to podiform chromite deposits where the chromite is coarse-grained (>1 mm), irregular, and anhedral in shape.)

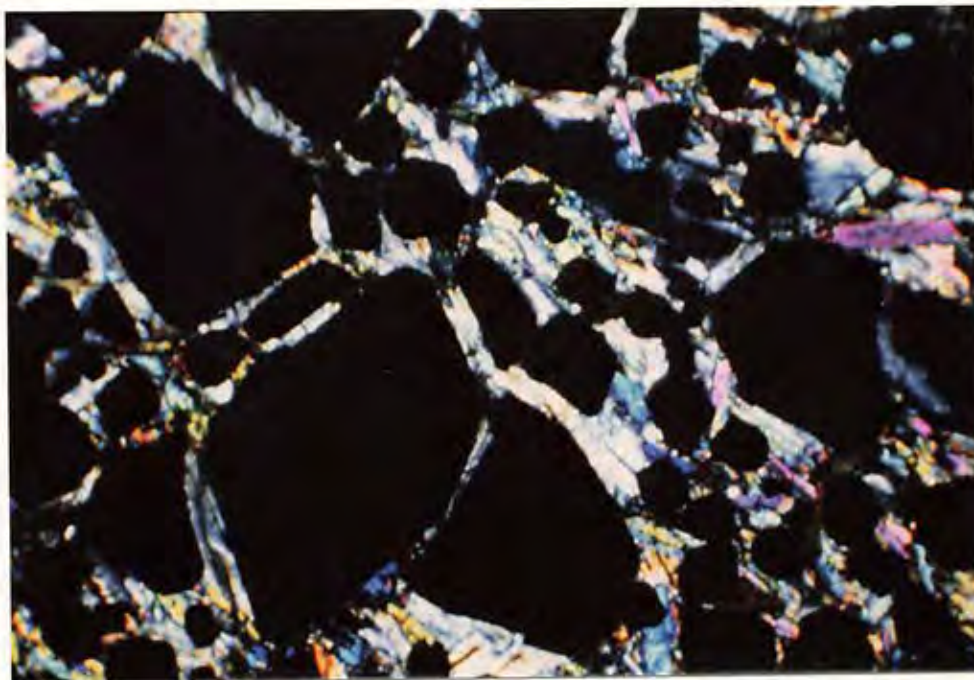


Figure 45. Sample # CB-AD-8530 (p. 5-37).
(Crossed nicols, field of view is
5 mm left to right) Chromite (dark rounded
grains) in a matrix of blady tremolite.
Chromite grains are unzoned and are 50%
 Cr_2O_3 by wt. (34 wt% chrome). See Appendix 4F.

Although the euhedral to subhedral granular chromite grains probably represent primary igneous chromite, the surrounding matrix is blady tremolite, indicating metamorphic recrystallization at greenschist facies conditions.

Minor mineralscarbonate

Carbonate was noted as a minor constituent (1-2%) in two anorthositic samples, and occurred both as fine veinlets and disseminated with actinolite and chlorite in the mafic areas of the sample.

opaque oxides

Very fine (50 - 200 μm) granular opaque oxides were noted along with the actinolite and hornblende assemblages in mafic areas of the samples. (See photomicrograph Figure 46, p. 159). Electron probe analysis of these oxides in one sample (E-1-B-8) showed they were Fe-oxides (magnetite by stoichiometric assumption, see Appendix 4-G). They normally constituted up to 2% of the mafic assemblages.

sulfides

Sample N-7(1)-18 (gabbroic anorthosite, p. 5-9) contained minor (<1%) sulfides and weathered sulfides, and minor small graphite flakes visible in hand specimen. Analysis for Platinum Group Metals (PGM) by fire-assay emission spectrography (Cooley et al., 1976) showed no PGM values at the limits of detection (detection limits: Pt = 0.005 ppm, Pd = 0.001 ppm, Rh = 0.002 ppm, Ru = 0.200 ppm, Ir = 0.100 ppm. Analysts: R. R. Carlson and E. F. Cooley,

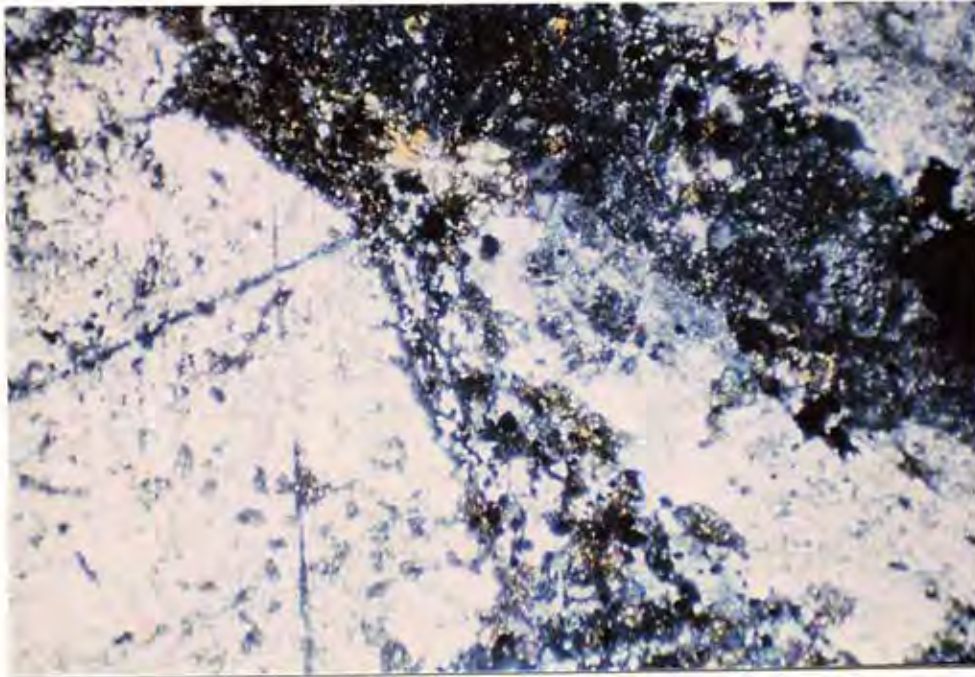


Figure 46. Sample #E-1-B-8 (p. 5-43)

(Plane polarized light, field of view is 5 mm, left to right.

Large lath-shaped plagioclase (white) is very strongly saussuritized and contains fine disseminated oxides (small dark spots). The measured plagioclase compositions ranged from An57 to An90 (a range of 33 mole % An), as opposed to the 1 - 5 mole % An variation common in most other cumulate plagioclase bearing samples (see Appendix 4-C).

Dark areas between the plagioclase grains are fine granular aggregates of hornblende and chlorite and quartz and opaque oxides.

Metamorphic recrystallization has progressed further in this sample than in most of the other samples showing euhedral, lath shaped plutonic plagioclases. (For example, see Figure 36, p. 139).

U.S.G.S., Denver). The thin section from Sample N-81-130, (troctolite, p. 5-34) contained 3 anhedral, multi-phase sulfide grains (up to 1 mm) of undetermined composition. These grains filled interstitial spaces as single grains between plagioclase grains and may be magmatic.

Samples E-1-B-8 and 13-81-227 contained minor Cu and Fe sulfides (<0.5% as very fine grains in the mafic metamorphic mineral aggregates (p. 5-43, 5-44, and Appendix 4-G). These appeared to be secondary (metamorphic) due to their intimate association with the granular mafic mineral aggregates.

Reaction Rims on Xenoliths (see also p. 130)

Reaction rims between the xenoliths and host intrusive were of two basic kinds:

- (1) Mafic - where amphibole in the xenolith was in contact with any of the host intrusive phases, the actinolite amphibole becomes darker green, strongly pleochroic, and coarser grained hornblende closer to the xenolith exterior (see Figures 40, p. 149, and 38, p.147). The dark green, strongly pleochroic amphiboles were generally higher in Al content than the lighter green non-pleochroic amphiboles (Figure 38, p. 147).

- (2) Felsic - glassy rims ranging in thickness from < 1 mm (Figure 47, p.162) to 5 mm (Figure 48, p. 163) were present on some of the cumulate textured xenoliths. These rims were higher in Si, Na, and K than either the xenolith as a whole or the host fine grained diorite for the two examples examined. The chemistry of two of these diffusion rims adjacent to plagioclase grains is listed in Appendix 4-E.

Non-cumulate Textured Xenoliths (Mineralogy)

The textures and mineralogy of the non-cumulate textured xenoliths are described in Appendix 5, pages 5-45 to 5-62. These include granular mafic amphibolites, amphibole-plagioclase schist, granites, gneiss, diabase and garnet.

Interpretation of Mineralogy (Cumulate Textured Xenoliths)

The mafic metamorphic mineral assemblages of actinolite ± hornblende ± chlorite in the xenoliths (as described in the previous sections) represent greenschist facies grade metamorphism of these basic igneous rocks, as defined by Best (1982, pp. 406-7). The presence of hornblende rimming some mafic domains might suggest a higher grade, but Deer et al. (1977, p. 164) state that actinolite in



Figure 47. Diffusion rim (bright band up center of photograph) on plagioclase grain (dark, on left) in contact with fine-grained diorite (right half of photograph).

Rims were higher in silica and alkalis than either the xenolith or the host diorite (Compare rim compositions, (Appendix 4-E) with compositions of fine-grained diorite and samples N-81-110 and NE-81-244 (Appendices 1-A and 1-C).)

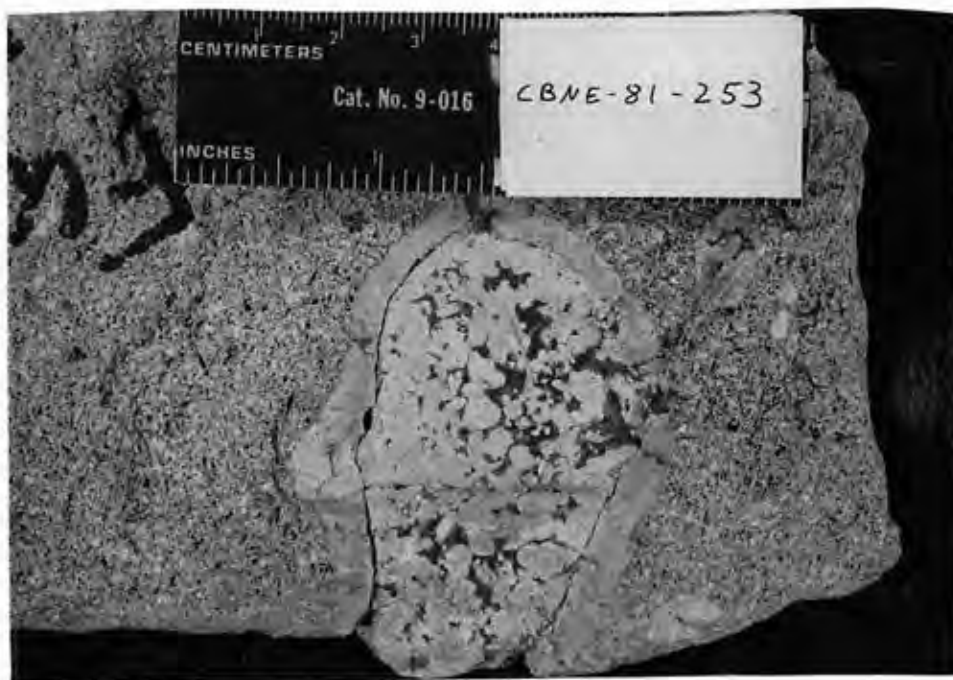


Figure 48. Thick (5 mm), glassy, felsic diffusion rim on gabbroic anorthosite sample (bottom center) in fine-grained diorite.

See Appendix 4-E for chemistry of diffusion rims on selected xenoliths.

association with chlorite, rimmed by hornblende, is a typical paragenesis of the greenschist facies.

Cumulus plagioclases in the xenoliths were largely unaffected by metamorphism (Figures 36, p.139 and 37, p.142).

Textures suggesting pseudomorphic replacement of original igneous mafic minerals were preserved (Figures 39, p.148 and 41, p. 151). Best (1982, p. 168) states that original fabric and mineralogical composition of gabbroic rocks can often be discerned because of pseudomorphic replacement of high temperature igneous minerals by lower temperature hydrous silicates. He notes that roughly isochemical replacement may aid in the identification of original mineralogical compositions.

The author believes that an attempt to define the original igneous mineralogy in the xenoliths is justified. The presence of cumulate textured calcic plagioclase (bytownite-labradorite), preserved intercumulus clinopyroxene, and pseudomorphic textures of mafic metamorphic mineral domains support a plutonic igneous origin for these rocks. Solid state metamorphic growth has not advanced far enough to obliterate magmatic grain boundaries in many of the xenoliths.

Fabrics of the mafic metamorphic minerals in the xenoliths are either randomly oriented (granular to blady)

aggregates, or have orientations that are constant within individual millimeter to centimeter size domains but differ between domains in the same thin section. This author believes that this isotropic fabric of metamorphic minerals resulted from hydrothermal metamorphism of the xenoliths in the host diorite melt, under hydrostatic conditions, because no preferred metamorphic fabric suggestive of earlier dynamic regional metamorphism is developed in the cumulate textured xenoliths.

Classification (Cumulate Textured Lithologies)

Silicate rock names used are those of the IUGS (Streckeisen, 1973), with the following conditions:

- (1) The cutoff for mafic minerals in anorthosite was set at 5% in order to emphasize the occurrence of intercumulus augite and/or calcic amphibole in the samples called gabbroic anorthosite (>5% mafics).
- (2) An attempt was made to identify cumulus igneous precursor minerals (based on the pseudomorphic textures and mineral compositions discussed on pp. 137 - 156.)
Rocks were called gabbro (cumulus plagioclase + calcic amphibole pseudomorphic after clinopyroxene); norite (cumulus plagioclase + chlorite plates pseudomorphic after ortho-

pyroxene); gabbronorite (calcic amphibole and chlorite pseudomorphic after clinopyroxene and orthopyroxene respectively); troctolite (magnetite - chlorite- amphibole after olivine); and chromitite (original chromite preserved), regardless of the proportions of the various cumulus phases present.

- (3) The prefix "mafic" denotes a specimen with mafic minerals > 50% by volume.

Questionable cumulate textured lithologies include mottled ultramafic to mafic lithologies with mafic mineral (amphibole and chlorite) domains that are possibly pseudomorphic after original igneous minerals (pp. 5-39 - 5-41), and two badly saussuritized plagioclase bearing lithologies (pp. 5-43 - 5-44).

The "Bronzite cumulate ?" xenoliths are specimens having a characteristic bronze-like schiller, composed of hydrous (serpentine group) minerals. This type of pseudomorphism is common after orthopyroxene (bronzite) cumulates and is referred to as "bastite" by Deer et al. (1977, p. 111; see Figure 50, p.168 this text).



Figure 49. A "banded" xenolith, showing white anorthosite (left), gabbroic anorthosite with dark intercumulus mineral (center, top to bottom of xenolith), and white anorthosite (right), in fine grained diorite.

Modal (rhythmic) layering in cumulate textured rocks is characteristic of layered basic intrusions (Carmichael et al., 1974, p. 461.)



Figure 50 . Altered ultramafic lithology composed of soft hydrous minerals. Specimen shows a bronze-like schiller across large areas of its surface when viewed in sunlight. Deer, et al. (1977, p. 111) state that complete alteration of orthopyroxene to serpentine pseudomorphs can produce specimens with a characteristic bronze-like luster known as "bastite". Ando et al. (1983) noted similar-appearing bastite pseudomorphs after orthopyroxene in harzburgites in ultramafic terrane of the Klamath Mountains, California.

Non-cumulate Lithologies (notes on classification)

The following lithologies are also listed (for xenoliths recovered from the Lodgepole Intrusion) in Table 5, p. 95 and Figure 22, p. 97. A brief definition of lithologic names used is provided here because their characteristics are not obvious from the assigned lithologic name alone.

Granular amphibolites are fine grained equidimensional-textured (hornblende/actinolite \pm biotite \pm chlorite) ultramafic to mafic amphibolites, with no preserved (either magmatic or sedimentary) fabric and up to 20% fine-grained ($\approx 300 \mu\text{m}$) feldspar.

Amphibole-feldspar schists have mineralogies like the granular amphibolites above, but the feldspar is arranged in stringers and the rock has a well-developed schistosity.

Diabase refers to a fine grained igneous rock having an ophitic texture of plagioclase in a mafic matrix. The dominant mafic mineral was hornblende in the one specimen studied in detail (p. 5-60).

Gneisses refers to medium to coarse grained foliated crystalline metamorphic rocks. Only two specimens (p. 5-57 and p. 5-58) were studied in detail. Most gneissic xenoliths noted in the field were of the quartz-feldspar \pm biotite variety illustrated on p. 5-57.

"Hornfels" refers to a fine-grained rock composed of a mosaic of equidimensional grains. None of the



Figure 51. Isoclinal fold in quartz-biotite-feldspar gneiss xenolith (top, center) in fine-grained diorite (host surrounding xenolith)

The well developed foliation, isoclinal folding, and observed mineral assemblage suggest that it may belong to the pre-2,700 m.y. group of gneisses (p. 36), because known younger rocks are not isoclinally folded.

specimens were studied in detail, but xenoliths noted were dense, dark green lithologies similar in appearance to the rocks of the Stillwater Complex contact aureole.

The Intrusive in Intrusive xenoliths noted for the Lodgepole Intrusion are interpreted as cognate xenoliths of dacite and diorite, possibly from the earlier intrusive phases of the multiple injection process which formed the Lodgepole Intrusion.

Maximum Country Rock Temperature at Contact of Coarse Porphyritic Dacite With Limestone

Samples of Threeforks Limestone in intrusive contact with the coarse porphyritic dacite border facies of the Lodgepole Pluton were collected from 1.2 km south of Clover Basin. Two carbonate samples, one from the contact (actually ≈ 2 mm away from the dacite in hand specimen) and one from three feet into the country rock were collected and subjected to Differential Thermal Analysis (DTA) and X-ray Diffraction (XRD) identification. The results are displayed in Appendix 8. No phases other than calcite were present in detectable amounts by XRD or DTA in either sample.

The fact that both samples showed intense, sharp endothermic peaks in the calcite decarboxylation range implies that even the sample closer to the intrusive contact

had not been heated past its decarboxylation temperature (924°C, at one atmosphere, for sample CBS-81-125-(C)) by intrusion of the coarse porphyritic dacite. Uncertainties involving the effects of pressure on decarboxylation and the actual heat conductivity across the intrusive contact (Jaeger, 1961) preclude the assignment of an exact magma temperature.

Summary of Results

A consideration of whole rock chemistry showed that the cumulate textured xenoliths represent basic igneous rocks with tholeiitic affinities. The span of sample average cumulus plagioclase compositions was An62 to An86. Minor intercumulus augite was preserved in some anorthositic specimens. Textures interpreted as pseudomorphic replacement of original cumulus clinopyroxene by calcic amphibole and cumulus orthopyroxene by chlorite occurred in some xenoliths. Comparisons of the cumulate textured xenoliths with Stillwater Complex outcrop lithologies are made in Chapter IV.

Chapter IV

Discussion

Source of Cumulate Textured Xenoliths

The cumulate textured xenoliths are tholeiitic in composition and show evidence of formation by crystal segregation (because the range of lithologies includes anorthosites, mafic-rich lithologies with minor cumulus plagioclase, and chromitites). The above features satisfy the criteria of Carmichael et al. (1974, p. 461) for rocks from layered basic intrusions.

The presence of northerly dipping layering in the outcrop of the basic stratiform Stillwater Complex 8 km south of the Clover Basin (Lodgepole) area (p. 49), as well as geophysical evidence (p.51), support a northerly continuation of the Complex at depth and suggest that it is the source of these cumulate textured xenoliths. An additional line of evidence is discussed below.

Comparison of Cumulus Plagioclase Bearing Xenoliths with Plagioclase Compositions of Raedeke (1982) and Hess (1960)

Table 10 (p.176) compares the sample average plagioclase compositions for cumulus plagioclase in xenoliths from the Lodgepole Intrusion against sample average cumulus plagioclase compositions measured by Hess (1960) and Raedeke (1982) from Stillwater Complex

outcrop samples. The sample average An(mole %) compositions for the suite of xenolith samples (An62-86) has a nearly identical span compared to Hess' (An63-86) and Raedeke's (An62-86) data for the Banded Series (Figure 11, p. 60, McCallum et al. column, reproduced in Segerstrom and Carlson, 1982).

If the xenoliths containing cumulus plagioclase are from the Stillwater Complex, they are almost certainly from the Banded Series (Figure 11, p.60, McCallum et al. column, reproduced in Segerstrom and Carlson, 1982) which contains abundant cumulus plagioclase. Raedeke, (1979, p. 49) reports rare cumulus plagioclase in the Ultramafic Zone, apparently < 1%, because it does not show on any of the modal diagrams in that text. The Basal Zone contains plagioclase, but cumulate textures are not prevalent (Raedeke, 1982, p. 105) and its thickness is minor, 152 m, (Page, 1977, p. 24), compared to the nearly 4500 m of exposed Banded Series (Raedeke, 1982, Plate V). Table 11 (p. 177) shows a stratigraphic column representing the thickness of the Stillwater Complex Banded Series cut into three sections based on cumulus plagioclase composition groups taken from Raedeke, 1982, Plate V. (The cutoffs are this author's choice - they do not correspond to Raedeke's zone divisions which are shown on Figure 11, p. 60). The percentage of Banded Series stratigraphy

Table 10

	An mole %		
	Lodgepole * xenoliths	Raedeke +	Hess ++
low (single sample average)	62	62	63
high (single sample average)	86	86	86

An (mole %) span for cumulus plagioclase, (values rounded to nearest whole number)

Source:

* Xenoliths

Figure 35, p. 138: low NE 81-1-2 = An 62.33
(electron microprobe)

high NE-81-244 (avg. of interior
and exterior thin sections,
same sample = An 86.12

+ Stillwater Complex Outcrop

Raedeke, 1982 Table A.1 low -Sample 161= An 61.88
(electron microprobe) Gabbrozone III #
Subzone

high-Sample 16 = An 85.59
Norite I
Subzone

++ Stillwater Complex Outcrop

Hess, 1960 fig. 25, p. 121

(optical and chemical low = An 63 (Exposed Top of
determinations) Upper Gabbro) #

high= An 86 (base of Norite Zone)

See Figure 11, p.60 for Raedeke's and Hess' Stillwater
Complex Stratigraphic Divisions

TABLE 11

Approximate cumulus plagioclase An mole % ranges	Height % of Banded Series Stratigraphy	N = number of xenolith samples from p. 138	% of xenolith samples = N + 22
4470 m An72-62 #	17%	3	14
3700 m An81-72 +	69%	9	41
635 m An86-81#*	14%	$\frac{10}{22}$ total	45

(From Raedeke (1982) Plate V
69 sample averages

#An decreases upsection in these intervals
*One sample average (An 78) is outside this range.
+An variable - no increasing or decreasing trends.

covered by each block is shown. The number of xenolith samples (from Figure 35, p.138) falling within each of the three An ranges is listed along with the percentage of the xenoliths from Figure 35 which it represents. The results show that the xenoliths appear to represent a widespread, if not strictly proportional, sampling of the Banded Series lithologies. The reader is cautioned, however, that individual samples in the Stillwater Complex commonly have a $\pm 1 - \pm 4\%$ range in An (Hess, 1960, p. 42), but even considering this variability there is evidence for samples from the upper (An62, 63) to lower (An 85, 86) (see p. 138, Figure 35) span of plagioclase compositions.

Based on the close agreement of the total span of measured plagioclase compositions (Table 10, p.176) between the Lodgepole xenoliths and Hess' (1960) and Raedeke's (1982) work, this author believes that the cumulus plagioclase bearing xenoliths represent lithologies brought up from the underlying Stillwater Complex.

Estimated Stillwater Complex Stratigraphic Positions of Selected Xenoliths

While there are general, broad lithologic and chemical trends in the Stillwater Complex (Hess, 1960; Raedeke, 1982), there are many small variations and stratigraphic complications that make it impossible to precisely place a random xenolith

in stratigraphic framework of the Complex. For example, while a nearly monomineralic anorthosite xenolith of An78 composition is "likely" to be from one of the three thick anorthosites of the Middle Banded Zone (Figure 11, p. 60 McCallum et al. column, reproduced in Segerstrom and Carlson, 1982), it may also be from some other than anorthosite layer in the Banded Series, or from a troctolitic layer where none of the widely scattered cumulus olivines happened to be sampled in that particular xenolith.

With the above cautions in mind, a few cases where xenolith compositions and textures merit an attempt at assignment to a narrower stratigraphic zone in the Stillwater Complex are proposed:

- (1) Two gabbroic anorthosites (N-81-102 , p. 5-12, An62) and (N-81-8720-A3, p. 5-13, An63), the latter of which contains large 10-15 mm plagioclase (as opposed to 3-7 mm "normal"), may be from the Upper Banded Zone (see (Figure 11, p. 60 McCallum et al. column, reproduced in Segerstrom and Carlson, 1982, alternatively called the "Upper Anorthosite" in the Carlson and Segerstrom column). Cumulus plagioclase compositions less than An65 are not reported in

lower anorthositic lithologies in the Stillwater Complex (Raedeke, 1982, Plate V).

- (2) A chromitite (CB-AD-8530), see p. 156) contains fine-grained (0.2 - 1.0 mm), euhedral, unzoned, cumulus chromite grains, and probably represents a Stillwater chromite from the Peridotite Member (Figure 11, p. 60, Page and Nokleberg column, reproduced in Segerstrom and Carlson, 1982) of the Ultramafic Zone. Jackson (1963, Table 1) lists Stillwater Complex chromite grain analyses up to 49.2 wt. % Cr_2O_3 . Loferski (1983, pers. comm.) has analyzed Cr_2O_3 compositions up to ≈ 52 wt. % in single phase chromite grains in segregated chromitite (interpreted as tectonically disrupted stratiform deposits) south of the Stillwater Complex near Red Lodge, MT., so this type of deposit in the basement gneiss complex cannot be excluded as a possible source, because chromite in the xenolith had a 50.16 wt. % Cr_2O_3 content.
- (3) If this author's interpretation of subhedral embayed, magnetic mafic assemblages as pseudomorphic after olivine (p. 153) is correct, then the troctolites (p. 5-32 to 5-35) are probably

from one of the five olivine bearing subzones in the Banded Series (Figure 11, p.60 , McCallum et al. column, reproduced in Segerstrom and Carlson, 1982) since these are the only cumulus plagioclase-rich zones which also contain cumulus olivine in the Stillwater Complex. Alteration of olivine is prevalent even in the Stillwater Complex outcrop.

- (4) Anorthosites (N-81-229, p. 5-3, An 82; N-81-160, p. 5-4, An 82; and N-81-500, p. 5-5, An 78) are likely to be from one of the three thick anorthosite units of the Middle Banded Zone (Figure 11, p.59, McCallum et al. column, reproduced in Segerstrom and Carlson, 1982) but lesser anorthosites having these plagioclase compositions do occur elsewhere in the Middle and Lower Banded Zones and cannot be ruled out here.

Comparison of Xenoliths from Lodgepole versus Enos Mountain/Susie Peak Intrusions

In every case where similar lithologies were available for comparison, the mean size of xenoliths

Table 12.
Mean size - xenoliths

Lithology	Enos Mt.	Susie Peak	Lodgepole
	(cm)	(cm)	(cm)
anorthosite	2.0	4.0	7.4
gabbroic anorthosite	4.7	3.3	7.2
gabbro	3.3	4.0	7.8
mafic gabbro	1.0	3.4	9.3
mottled and ultra-mafic/mafic rocks	2.6	1.8	5.0
diabase	1.8	2.0	4.9
amphibole-plagioclase schist	2.0	—	4.6
granular amphibolite	2.0	1.6	4.2

Comparison of xenolith sizes for similar lithologies from the Enos Mountain, Susie Peak, and Lodgepole intrusions.

from the Lodgepole Intrusion was larger than the mean size of xenoliths from Enos Mountain and Susie Peak intrusions (see Table 12, p. 182).

The largest cumulate textured xenoliths found in each intrusion were a gabbro, 31 x 31 x 18 cm (NE-81-244) from Lodgepole, a 9 cm (largest dimension) gabbro from Enos Mountain, and a 9 cm (largest dimension) gabbro from Susie Peak.

Four hypotheses for the xenolith size differences discussed above are considered here.

(1) The smaller mean sizes and smaller maximum sizes for xenoliths of similar lithology may imply a deeper source (hence greater depth to the Stillwater Complex) for cumulate textured xenoliths from the Enos Mountain and Susie Peak intrusive areas. Although gravity data (Bonini, 1981; see p.51 this report) suggest that the Stillwater Complex is flat-lying in the subsurface further north of the Enos Mountain - Susie Peak area under the Crazy Mountain Basin, the decreasing xenolith sizes suggest that depth to the Complex increases between the Lodgepole Intrusion and the Enos-Mountain-Susie Peak areas.

(2) Alternatively, the smaller sizes of similar xenolith lithologies may reflect a greater horizontal distance of xenolith transport, if some of the intrusions hosting the xenoliths in the Enos Mountain - Susie Peak

area were low angle dike-like offshoots from the main Lodgepole Pluton.

(3) The smaller xenolith sizes in the Enos Mountain and Susie Peak areas may reflect a slower ascent rate for these two intrusions (compared to the Lodgepole Pluton) with more time for xenolith assimilation. However, a slower, less forceful rate of intrusion for Enos Mountain magma is contradicted by the large size of cognate xenoliths (volcanic clasts up to 2 m in diameter, p.116) it contains.

(4) The difference in xenolith size may be an artifact of the sampling scheme.

With the data available, only the third possibility above can be considered unlikely.

Implications for the Upper Hidden Zone

The total span of cumulus plagioclase compositions measured in the xenoliths (Figure 35, p. 138) raises questions about the nature of the Upper Hidden Zone of the Stillwater Complex (unfortunately, primary cumulus ferromagnesian minerals in the xenoliths have been altered to hydrous minerals and can not be used predict fractional crystallization trends (p. 135).

Hess (1960, p. 101) predicted the existence of a

stratigraphically higher Hidden Zone beneath the Paleozoic unconformity north of the Stillwater outcrop (p. 44). He based his estimate on a consideration of the composition of "chill margin" rocks taken to represent the original Stillwater "magma" composition and the composite composition of the exposed Complex, (i.e., what has been "subtracted" from the "magma" composition).

He predicted the existence of a Hidden Zone equal to 40% of the total Complex thickness consisting of lithologies enriched in iron and alkalis (quartz-bearing ferronorite bulk composition for the zone), similar to the rocks of the exposed portion of the Skaergaard Intrusion, minus olivine.

If the exposed Stillwater Complex stratigraphic thickness of 4935 m (Hess, 1960, p. 103) is used, then a "Hidden Zone" 3290 m thick (= 40% of total Complex thickness) would be predicted by Hess' model as illustrated in Figure 52 (p. 187,).

Using an average Stillwater Complex compositional layering dip of 60° N for the Banded Series in the area of Picket Pin Mountain (from p. 49) and assuming a constant average dip discordance of 30° between Stillwater layering and the Cambrian Sediments (reasonable for the Picket Pin unconformity, see map, Plate I and p.44), the model (p. 187) shows that, by the time the area of the central

diorite intrusive phase (containing abundant cumulate textured xenoliths with a span of cumulate plagioclase compositions An62 - An86) of the Lodgepole is reached 8 km to the north, there should be enough "room" for a Hidden Zone equal to 40% of the Complex thickness to exist in the basement under the cover of Cambrian sediments. (however, it is more likely that the Hidden Zone, if it exists, is \leq 2,000 m thick, as discussed on p.194.

Using Hess' (1960, p. 105) normative mineral averages for the composition of the Hidden Zone, Bonini (1981) calculated an average density of 3.03 gm/cm³. Using the same reasoning, xenoliths had densities calculated from the normative mineralogy (see Appendix 7) of up to 3.20 gm/cm³, with 7 xenoliths having calculated densities \geq 3.03 gm/cm³ and 4 more \geq 3.00 gm/cm³. Therefore, xenoliths of equal or greater density than the Hidden Zone average were raised in the Lodgepole magma.

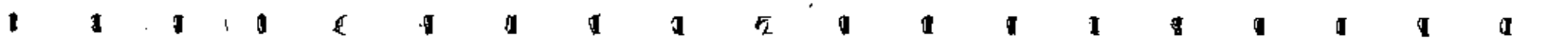
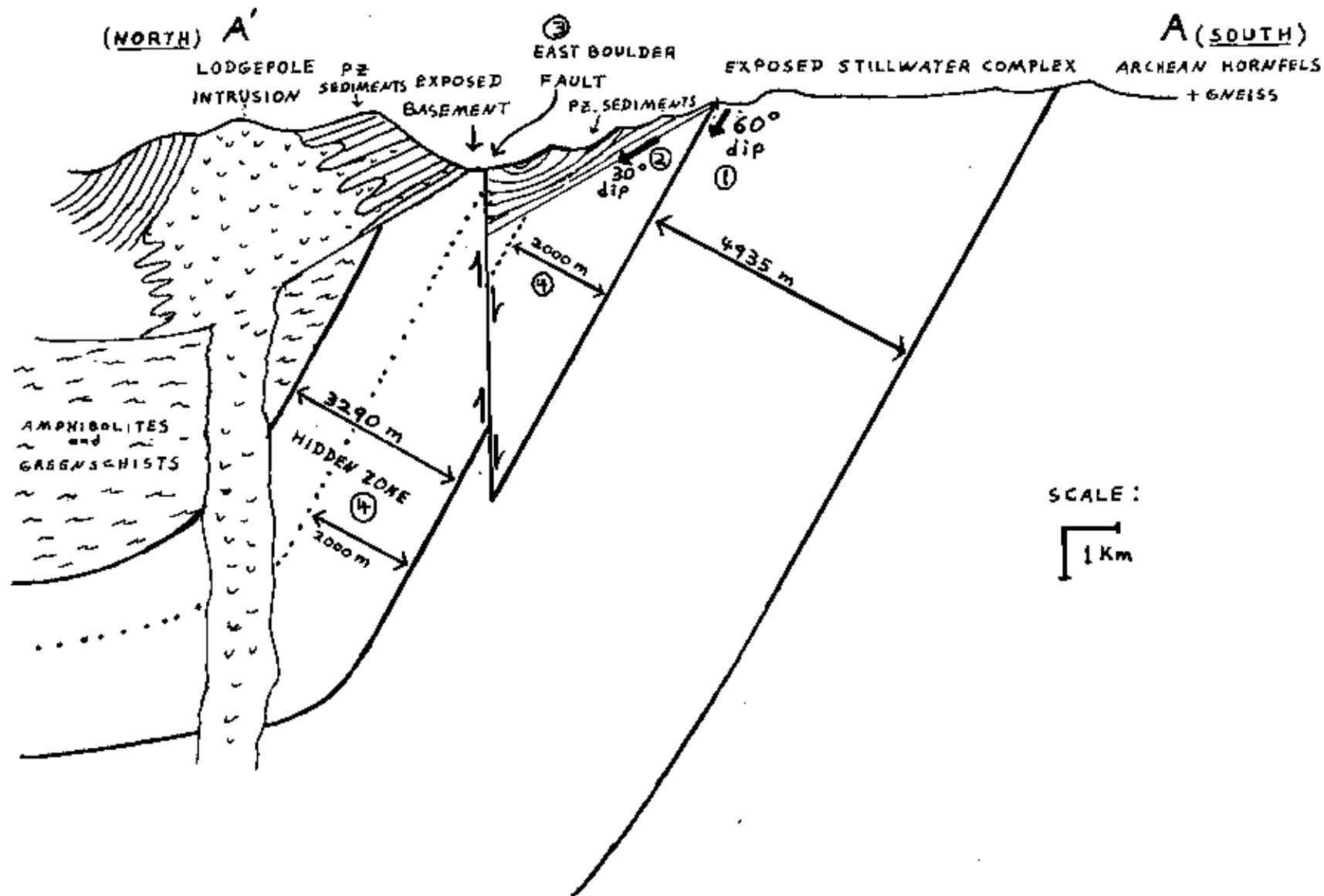
As discussed on p. 178 the xenoliths collected appear to represent a widespread sampling of lithologies, with samples from the Ultramafic Zone (chromitite) the Middle Banded Zone (An72-81 cumulus-plagioclase rich lithologies), and the Upper Banded Zone (gabbroic anorthosites An62-63). Hess' (1960, p. 103) normative composition estimate for the Hidden Zone is still relatively plagioclase rich

Figure 52. Structure model for Stillwater Complex assuming:

- (1) 60°W dip of compositional layering throughout Complex. Exposed Complex = 4935 m, Hess (1960, p. 103) (=60% of total Complex thickness).
- (2) 30° N dip of middle Cambrian unconformity
- (3) High-angle East Boulder Fault, north side up, 1200 m vertical throw (early Tertiary movement).
- (4) Hidden Zone of Stillwater Complex:
3290 m = Hess (1960, p. 103) (= 40% of total Complex thickness)

2000 m = proposed maximum Hidden Zone thickness if structure attitudes in (1) (2) and (3) above are used.

See text, p. 192 for discussion.



(51.29 wt. % plagioclase) with an average normative An content of 53 mole %. Hess states (1960, p. 100) that the normative and modal plagioclase compositions for the Exposed Complex above the Ultramafic Zone agree closely, so we might expect the same to hold true for the Hidden Zone.

Therefore, based on the structural geology model (Figure 52, p.187) and Hess' compositional and thickness estimates for the Hidden Zone, and assuming at least a crudely proportional sampling of the Complex (which seems reasonable from the discussion, p.174) by the Lodgepole magma, we should expect to see xenoliths with cumulus plagioclase compositions \leq An 53 in about half (since this is the average for the Upper Hidden Zone) of any Hidden Zone xenoliths. Because Hess' postulated Hidden Zone thickness (3290 m) is equal to about 78% of the thickness of the Exposed Complex excluding the Ultramafic Zone (4935 m exposed total - 762 Ultramafic Zone = 4173 m ; i. e., 3290 m (Hidden Zone) / 4173 m (Exposed Complex = 0.78), we should expect to see at least a few, perhaps 4 or 5 out of the 22 plagioclase sample averages, with values \leq An 53. (The number of such "Hidden Zone" xenoliths might be expected to be less if the Hidden Zone is thinner).

Based on measured sample average plagioclase compositions, no compositions $< \text{An } 62$ were found in any of the cumulate textured plagioclase-bearing xenoliths, except for one badly altered sample (13-91-227, An 47.28) with an extremely erratic (An 29.72 \rightarrow An 57.63, range = 27.91 mole % An) range of measured plagioclase composition (this sample is not included in Figure 35, p. 138).

A number of possible explanations can be offered as to why no obvious Hidden Zone compositions were found:

(1) Inadequate or unrepresentative sampling in this study.

(2) A Hidden Zone of Hess' estimated composition did exist but was eroded after intrusion of the Complex (2,701 m.y., p. 38) but before Middle Cambrian time (p.45) when the Complex was tilted $25^{\circ} - 35^{\circ} \text{ N}$.

(3) Hidden Zone samples may have been mineralogically altered. Two strongly saussuritized plagioclase-bearing samples exhibit metamorphic recrystallization textures and highly variable plagioclase compositions. Not only do they show iron- and alkali- enrichment with respect to the other xenoliths analyzed but they also exhibit possible relict cumulate textures (see Figure 31, p.126, and Figure 46, p. 159). However, there are no petrologic reasons why Hidden Zone xenoliths would be preferentially altered relative to other Stillwater lithologies.

(4) Sampling of the Complex by the Lodgepole magma was not even approximately representative, skipping the Hidden Zone entirely. This does not seem likely considering the span (An62 - An86) in plagioclase compositions encountered in the xenoliths (p. 177).

(5) The "chilled margin" composition assumed by Hess to represent the magma composition, may have been contaminated by assimilation of the low-melting components of the hornfels (p. 37) floor rocks. Raedeke (1982, p. 105-113) presents evidence that the Stillwater magma near its liquidus would cause partial melting of the hornfels due to the initial heat of the magma plus the latent heat of crystallization released on cooling of the magma. Barker (1975) shows that hornfels inclusions in the Stillwater Basal Series (McCallum nomenclature, Figure 11, p. 60) were depleted in their low melting components relative to the average footwall hornfels. This would suggest that Hess' chilled border sample was contaminated, and may have been enriched in sodium and potassium leaving the plagioclase compositions in his predicted Hidden Zone too Ab rich after subtracting the exposed Stillwater Complex average.

(6) The Stillwater Complex was formed in such a manner that fractional crystallization did not occur. However, Raedeke's (1982) work has shown that the Ultramafic

Zone, Lower Banded Zone and Upper Banded Zone appear to have formed from one magma suite (although the Middle Banded Zone was formed from a suite of magmas of distinctly different composition). The decrease in plagioclase An compositions from An86 at the base of the Lower Banded Zone to An62 at the top of the Exposed Complex (Raedeke, 1982, Plate V) suggest that fractional differentiation did occur.

(7) More differentiated material may have been tapped from the magma chamber by volcanic eruptions.

Except for the arguments stated against (3), (4), and (6) above, the author can find no reasons to rule out any of the other hypotheses.

Economic Resource Possibilities

A chromitite xenolith (p. 156 and p. 5-37) suggests that chromite horizon(s) continue in the Stillwater Complex under the Lodgepole Intrusive area.

The presence of anorthositic (An 82-83, p. 5-3, 5-4, 5-8) and troctolitic (An 79-82, pp. 5-32 to 5-35) lithologies in xenoliths having plagioclase compositions similar to the Olivine Bearing Subzone I (Raedeke, 1982, Plate V) which contains the Johns-Manville Platinum Group Metal (PGM) horizon suggests, at least, that favorable

lithologies continue northward at depth under the Lodgepole area. Except for one sample (N-7(1)-18, p. 5-9) no analysis for PGM's was carried out. The presence of magmatic-appearing (primary) interstitial sulfide in samples N-7(1)-18 (p. 5-9) and N-81-130 (p. 5-34) suggest that at least minor sulfide precipitation did occur in the northern extent of the Complex.

No primary (i.e., cumulus or poikilitic textured) magnetite or vanadiferous magnetite was found in any of the xenoliths. (Many xenoliths contained minor secondary opaque oxides that were almost certainly alteration products of primary ferromagnesian minerals (see Figure 46, p. 159, and p.158).) The absence of lithologies more differentiated (as judged by a decrease in measured cumulus plagioclase An content) than known Stillwater Complex rocks does not suggest the presence of an iron- and alkali- enriched Hidden Zone. Maze and Carlson (1981), however, report Fe-Ti oxides interstitial to cumulus plagioclase which constitute up to 1 - 2 % of the coarse-grained anorthosites in the uppermost exposed layers of the Stillwater Complex north of Picket Pin Mountain.

Structural Constraints on Depth to Stillwater Complex

A simple structural model along the A - A' portion of the Plate III Cross-section is illustrated in Figure

52. (p. 187). (Because the northward-sloping ramp-type nature of the Beartooth Front in the area north of Picket Pin Mountain is much different from the overthrust-to-the-north nature of the Front further east (p. 58) where Bonini's (p. 54) gravity cross-section model line is constructed, no attempt is made to use this gravity cross section model to directly estimate a depth to the Complex beneath the Lodgepole area. However, Bonini (pers. comm.) estimates the Complex flattens at depth north of most of its outcrop belt so a general flattening is shown in Figure 52 (p. 187) under the Clover Basin (Lodgepole) area.)

Stratigraphic thicknesses used in the following discussion are from Hess (1960, p. 103). Using the structural attitudes shown in Figure 52, p. 187 (reasons were given previously, p. 185) and a Hess-model Hidden Zone equal to 40% of the total Stillwater Complex thickness, would imply that any basement (beneath the middle Cambrian sediments) exposed on the north side of the East Boulder Fault (assumed high-angle, see p. 48) should be Stillwater Complex. However, the only basement exposed north of the East Boulder Fault are mafic amphibolites and greenschists (a small area south of the Lodgepole Intrusion, and a large band beginning \approx 3 km further west (see Plate I, "PGs").

There are two likely end-member reasons for the exposed "non-Stillwater" basement seen north of the East Boulder Fault:

- (1) The East Boulder Fault may be lower-angle than its surface expression indicates, and southward movement at the north block may have moved amphibolites and greenschists to their present position from ≥ 1.5 km to the north (This distance is necessary if the 40% Hidden Zone thickness, and if Stillwater Complex dips $\leq 60^\circ$ are used in the model).

and/or

- (2) The Hidden Zone thickness may be less than the 3290 m (= 40% of total Complex) that Hess estimated. (note: from Figure 52, p. 187 that if the Hidden Zone were ≤ 2000 m thick, non-Stillwater basement could be exposed north of the East Boulder Fault even if the fault is nearly vertical (as proposed on p.46).)

At any locality immediately north of the East Boulder Fault, upper horizons of the Stillwater Complex could exist under a thin cover of the exposed amphibolites and greenschists, if the Hidden Zone were ≈ 2000 m thick, or the upper horizons could be as deep as 6 km (from Figure 52, p. 187) if there is no Hidden Zone.

Figure 53 (p.196) illustrates the geometry of a proposed drill site location that should maximize the chance of intersecting higher stratigraphic horizons in the Stillwater Complex.

A location at an elevation of 2286 m (7500 ft. on Plate I, Map) along Blacktail Creek (3.7 km NNE of the Peak of Picket Pin Mountain) would be 1.4 km NE of the nearest exposed Stillwater Complex (see Figure 11, p.60 Upper Anorthosite of Segerstrom and Carlson nomenclature). According to Page et al., (1973, U.S.G.S. Mount Douglas Quadrangle Geologic Map), this location is in the Cambrian sedimentary section stratigraphically below the Bighorn Dolomite. Using Garbarini's (1957) maximum section thicknesses, stratigraphic thickness distance to basement (below the lowest middle Cambrian sediments) should be 350 m, assuming no repetition of section.

A drill hole at this location could serve as a test to see if there is a substantial thickness of Hidden Zone. A 60° dip of layering in the Complex would mean that a drill hole should intersect Stillwater Complex representing a horizon 0.7 km stratigraphically higher in the Complex than is presently exposed, at a stratigraphic distance of 350 m through the Cambrian sediments.

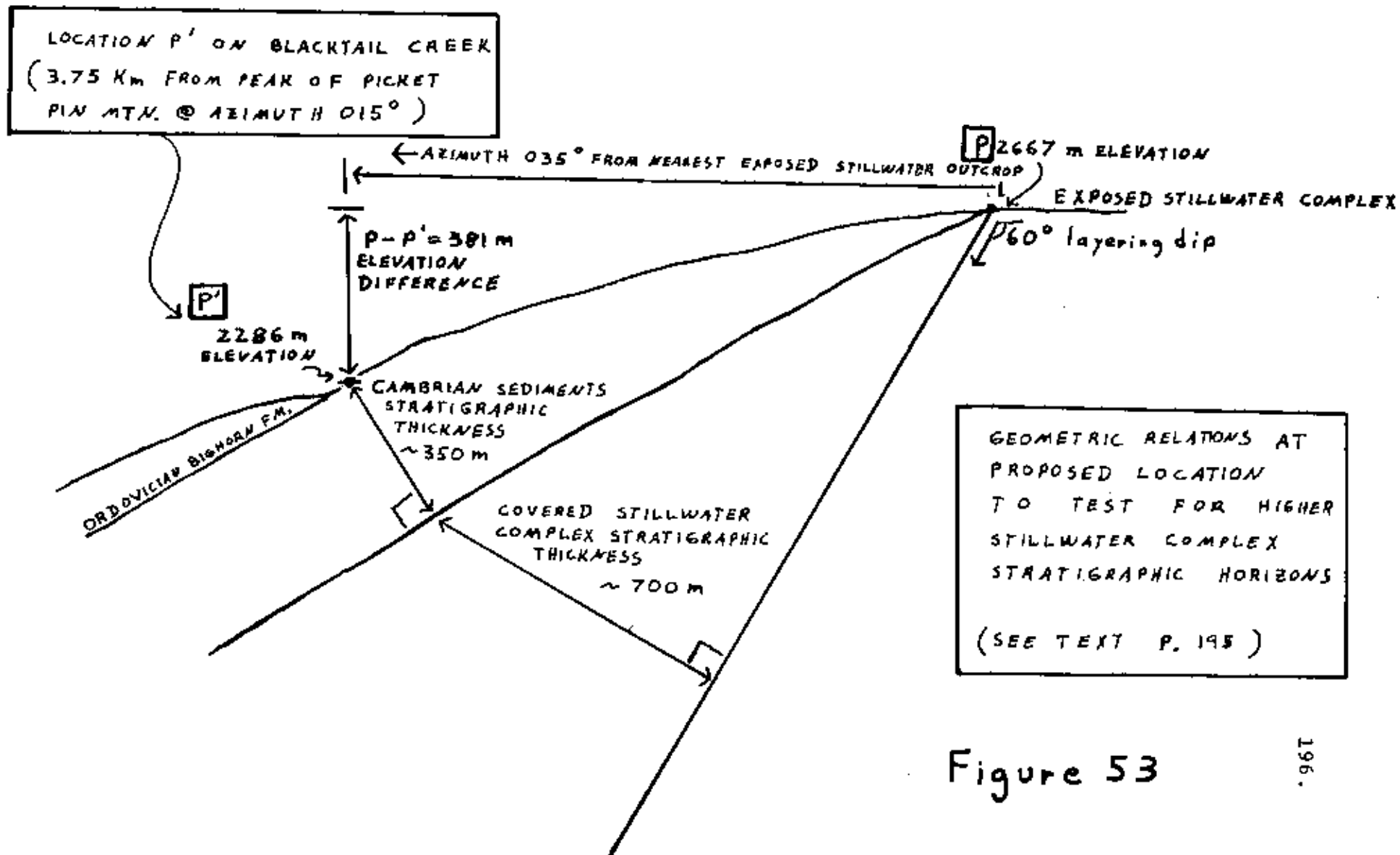


Figure 53

If the basement intersected is not Stillwater Complex (i.e., amphibolites and greenschists or other lithologies), this would imply that a Hidden Zone thickness < 0.7 km thick is present north of the exposed Stillwater Complex at that location.

A second drill site anywhere within the belt of greenschists and amphibolites north of the East Boulder Fault (PGs, Plate I) can be suggested. Because the greenschists and amphibolites represent exposed Precambrian basement on the upthrown north side of the Boulder Fault, upper layers of the Stillwater Complex might lie beneath a thin cover of these lithologies, if the East Boulder Fault is high angle and if the Hidden Zone is ≈ 2000 m thick (see p. 192).

Information gained from the above drill holes could help constrain a depth to any northern extent of the Stillwater Complex and aid in assessing the reserve potential of any ore mineralization that might be encountered within mineable (< 3 km) limits.

Estimation of Lodgepole Magma Ascent Rates from a Consideration of Xenolith Settling Velocities in the Magma

A range of possible settling velocities for the xenoliths in an andesitic melt (compositional equivalent of diorite) were considered in an attempt to constrain some minimum necessary ascent rates for the magma which formed the fine-grained diorite of the Lodgepole Intrusion in the Clover Basin area. Two extreme cases, as discussed below, were used to represent andesitic magma above its liquidus (Case 1) and a 50% crystalline andesite magma (Case 2). Settling rates for the xenoliths would be minimum ascent rates for the magma which carried the xenoliths, because the actual magma ascent rate would have to have some additional net upward component above what was necessary to counterbalance the xenolith's gravitationally driven descent.

A Stoke's Law solution was used as a first approximation of the settling velocity of the xenoliths in the magma:

$$v = \frac{2}{9} g r^2 \frac{\rho_s - \rho_L}{\eta}$$

where: v = settling velocity (cm/sec)
 g = 980.1018 cm/sec²
 r = radius of xenolith
 ρ_s = xenolith density (from Appendix 7)
 ρ_L = magma density for andesitic magma
 η = magma viscosity, poises

Densities of the large cumulate textured xenoliths (from Appendix 7) were used, and the radii of spheres of equal

volumes to the calculated volumes of these two large cumulate xenoliths (p.92) were used:

$$\text{NE-81-245 } \rho_s = 2.90 \quad r = 14 \text{ cm}$$

$$\text{NE-81-244 } \rho_s = 3.05 \quad r = 16 \text{ cm}$$

In Case 1, an andesitic magma was assumed to have a $\rho_L = 2.49$ and $\eta = 180$ poises (for a Crater Lake andesite, 2.63 wt. % H_2O , Pressure = 7.5 Kb, Temperature = 1175°C , about 50° above the experimental andesite liquidus under the stated P-T conditions; data from Kushiro, 1978, Figure 16, p. 276). This appears to be a reasonable maximum depth of Stillwater xenolith entrainment and minimum viscosity for the Lodgepole magma for two reasons:

(1) Assuming a continued 60° dip for the Stillwater to the north, its lower layers would lie at a depth of ≈ 24 km under the Lodgepole area, which would correspond to a pressure (using a gradient of 0.3 Kb/km) of ≈ 7.2 Kb, which is close to Kushiro's 7.5 Kb value above.

(This depth is unlikely, because geophysical evidence (p.51) indicates that the Complex flattens to the north at depth, but is used here simply as some maximum depth at which the Lodgepole magma might have begun to entrain Stillwater Complex xenoliths).

(2) The viscosity above is for an andesitic melt above its liquidus. This figure must be taken as a minimum viscosity; it probably was greater because the Lodgepole fine-

grained diorite is actually about 50% phenocrysts. However this minimum viscosity should allow for the maximum xenolith settling rates, since from the Stoke's Law equation V is inversely proportional to η , and η would increase as the magma crystallized.

Using the Case 1 values of $\rho_L = 2.49$ and $\eta = 180$ poises the maximum settling rates for the xenoliths would be 97 cm/sec for NE-81-245, and 173 cm/sec for NE-81-244. Taking the larger of the two settling rates above, the Lodgepole magma would have had to rise at a rate of at least 1.73 m/sec, (or at 1.73 m/sec x 3600 sec/hr. \approx 6200 m/hr.), plus some additional upward magma velocity to give the xenoliths a net upward velocity.

In Case 2, the Lodgepole magma was assumed to have a $\rho_L = 2.65$ gm/cm² (i.e., \approx 5% less than the solid density of 2.79 gm/cm² calculated from the normative mineralogy for fine-grained diorite sample AD-8380). A $\eta = 10^{12}$ poises was used (from Shaw, 1969, for a basalt that is 50% crystalline. The Lodgepole diorite is \approx 50% phenocrysts, and its η at that crystallinity would probably be somewhat higher than 10^{12} poises, because it is more siliceous than a basalt.

Using the Case 2 values ($\rho_L = 2.65$ gm/cm², $\eta = 10^{12}$ poises), settling rates for the two xenoliths were calculated as 1×10^{-8} cm/sec (for NE-81-245) and 2.2×10^{-8} cm/sec (for NE-81-244), or only 7.92×10^{-5}

cm/hr even for the denser (NE-81-244) xenolith. In Case 2 the magma ascent rate could therefore be very slow and still raise the xenoliths.

Assuming even the minimum likely magma viscosity and magma density (Case 1), the necessary upward magma velocity required to counterbalance xenolith settling ($= 1.73$ m/sec for Sample NE-81-244) is not rapid.

Case 2 illustrates that in a Lodgepole magma that was 50% phenocrysts, even the denser of the two xenoliths (NE-81-244) would have almost no tendency to settle in the magma ($\approx 2.2 \times 10^{-8}$ cm/sec., or $\approx 8 \times 10^{-5}$ cm/hr).

Using a viscosity of 31,200 poises (for an andesitic basalt at 1200° C from Motomura, Japan, as summarized in Clark, 1966, Table 12-8, p. 299) and a density of 2.65 gm/cm³ (as in Case 2 above), a settling velocity for the denser xenolith (NE-81-244 = 3.05 gm/cm³) intermediate between the Case 1 and Case 2 values above can be calculated as 0.71 cm/sec, or ≈ 26 m/hr.

Although the hypothetical conditions outlined in Case 1 and Case 2 define the minimum necessary ascent rates (required to raise the xenoliths) for an andesitic magma above its liquidus and for a 50% crystalline magma, it is not possible to define the actual magma ascent rate from the above parameters.

Several empirical factors, however, suggest a rapid ascent rate for the Lodgepole (fine-grained diorite) magma:

(1) Many angular xenoliths were found (p.95) suggesting that a short time was available for digestion of the xenoliths in the melt. The degree of rounding (p. 95) for the majority of the xenoliths lithologies is not great (i.e., most xenolith lithologies were not dominantly "rounded").

(2) Except for the ultramafic lithologies, most of the xenoliths in a given class did not exhibit well developed reaction or assimilation rinds (such as illustrated in Figure 48, p. 163).

(3) The aphanitic groundmass of the central fine-grained diorite phase of the Lodgepole suggests that it completed its crystallization rapidly at a shallow depth (\approx 2000 m, p. 81).

(4) The abundance of angular, fragmental, volcanic clasts in the breccias of the Enos Mountain and Susie Peak areas suggest that the late Cretaceous (pp. 103 and 107) volcanism and intrusion of dacitic and andesitic magmas were forceful emplacement events.

Several empirical factors, however, suggest a rapid ascent rate for the Lodgepole (fine-grained diorite) magma:

(1) Many angular xenoliths were found (p.95) suggesting that a short time was available for digestion of the xenoliths in the melt. The degree of rounding (p. 95) for the majority of the xenoliths lithologies is not great (i.e., most xenolith lithologies were not dominantly "rounded").

(2) Except for the ultramafic lithologies, most of the xenoliths in a given class did not exhibit well developed reaction or assimilation rinds (such as illustrated in Figure 48, p. 163).

(3) The aphanitic groundmass of the central fine-grained diorite phase of the Lodgepole suggests that it completed its crystallization rapidly at a shallow depth (\approx 2000 m, p. 81).

(4) The abundance of angular, fragmental, volcanic clasts in the breccias of the Enos Mountain and Susie Peak areas suggest that the late Cretaceous (pp.103 and 107) volcanism and intrusion of dacitic and andesitic magmas were forceful emplacement events.

Chapter V
Summary and Conclusions

SUMMARY AND CONCLUSIONS

The following conclusions are offered, based on an integration of the field and laboratory data:

- (1) Northerly dipping compositional layering (50° - 70° N; Segerstrom and Carlson, 1982) in the central and western portions of the Stillwater Complex, as well as gravity data (Bonini, 1981) suggest that this 2,700 m.y. layered intrusive Complex extends northward beneath the middle Cambrian unconformity which defines the upper exposed boundary of the Complex. This unconformity represents more than a 2,000 million year interval and a structural discordance of 20° - 30° between the upper layers of the Complex and the overlying middle Cambrian shales. An unknown thickness of Hidden Zone (Hess, 1960) of the Complex, and possibly some of its roof rocks, are likely to exist as the first crystalline basement beneath the middle Cambrian units to the north.

If the East Boulder Fault is high angle as its surface expression would suggest, and, if this Hidden Zone extended the Stillwater Complex stratigraphic column by 40%, then Stillwater Complex lithologies should have been exposed on the north side of the East Boulder Fault (Figure 52, p.187). The fact that the exposed Precambrian basement north of the East Boulder

Fault is foliated amphibolites and greenschists, and not cumulus textured Stillwater type lithologies, suggests that the Hidden Zone of the Complex (if it exists) is probably less than 2,000 m in stratigraphic thickness. (See also conclusion number 6, p. 207).

- (2) The 25° to 70° northerly dips of the Paleozoic sediments along the Beartooth Front in the area north of the central portion of the Stillwater Complex between Picket Pin Mountain and the Main Boulder River contrast markedly with the vertical-to-overthrust to the north-and-east nature of the Paleozoic strata along the perimeter of the uplifted Beartooth Block elsewhere along its northern and eastern boundaries. The above relations suggest that the Stillwater Complex may have acted as a resistant strut in the basement during the main Beartooth uplift, preventing a northward overthrusting of the uplifted block.
- (3) The general parallelism of a WNW-ESE trending, northerly dipping foliation in the amphibolites and greenschists (exposed below the middle Cambrian sediments north of the East Boulder Fault) with the latest foliation (1600 - 1800 m.y., pp. 38-39) in the Stillwater Complex to the south suggests that these amphibolites and greenschists either represent roof rocks to the northerly dipping Stillwater Complex, or, at a minimum, that they